Investigation of the Stability of Fumed SiO_2 / Metal Oxides (*MO* = Al_2O_3, TiO_2) under Harsh Hydrothermal Conditions

by

Müjde Yahyaoğlu

A Thesis Submitted to the

Graduate School of Sciences & Engineering

in Partial Fulfillment of the Requirements for

the Degree of

Master of Science

in

Materials Science and Engineering

Koç University

August 2017

Koç University

Graduate School of Sciences and Engineering

This is to certify that I have examined this copy of a master's thesis by

Müjde Yahyaoğlu

and have found that it is complete and satisfactory in all respects,

and that any and all revisions required by the final

examining committee have been made.

Committee Members:

_____

Prof. Dr. Mehmet S. Somer (Advisor)

_____

Assoc. Prof. Uğur Ünal

_____

Assoc. Prof. Güldem Kartal Şireli

Date: _____

ABSTRACT

Fumed metal/metalloid oxides, FMO (such as alumina, titania, silica etc.) are important raw materials for various industrial applications from chemical industries to food technologies. Due to extensive use of fumed SiO_2 as a carrier in pharmaceutical applications, catalysis applications, cracking petrochemicals, and conversion for production of bio-renewables, hydrothermal stability is a critical requirement. Fumed silica based materials have high specific surface areas in the range of 50 and 400 m^2/g which allows an efficient dispersion of active sites and large pore volume that favours the diffusion of bulky molecules in catalysis applications, however, their applications are limited by their poor stability due to the hydrolysis of their surfaces. Therefore; the research on developing hydrothermally stable mesoporous materials for catalytic applications has gained interest. To improve the hydrothermal stability of SiO_2, many different methods are used such as adding salt, increasing pore wall thickness, and incorporating heteroatoms in situ or by post treatments.

In the present study, the stability of fumed SiO_2 materials and composites produced by flame hydrolysis is investigated under hydrothermal conditions applied for 24 hours and 7 days. Specifically, pure fumed silica, fumed alumina, and binary fumed mixed oxides of Al_2O_3- and TiO_2-doped silica samples with various doping percentages are used for hydrothermal treatment. Surface areas of all untreated and hydrothermally treated samples are calculated by Brunauer-Emmett-Teller (BET) analysis and pore volume & pore maximum are calculated by Barrett-Joyner-Halenda (BJH) analysis by using nitrogen adsorption method. After hydrothermal treatment, BJH pore volume analysis shows decreases of 98 % for pure alumina, 75 % for pure silica and 26 % for Al_2O_3-doped silica in the pore volumes, respectively. According to powder X-ray Diffraction (XRD) analysis, all of the samples maintained their amorphous structure after the treatment. BET analysis indicates that after hydrothermal treatment, pure alumina and pure silica reveal the highest BET surface area reduction by 92 and 83 %, respectively. On the other hand, incorporation of Al_2O_3 and TiO_2 into the silica matrix enhanced the surface stability and minimize the surface area reduction. Moreover, as doping amount increases (e.g. 0.8 to 1.0 wt %) the surface of the materials becomes more stable. Comparison of 1.0 % Al_2O_3- and TiO_2-doped silica samples shows that incorporation of Al_2O_3 and TiO_2 stabilizes the structure yielding BET surface area reduction by 31% and 26 %, respectively. The trend of surface area stabilization by doping follows the order: TiO_2-doped silica > Al_2O_3-doped silica > pure silica. Titanium is a more electropositive dopant than

aluminum and silicon itself and it has a higher affinity to the electrons of surface OH^- groups. Therefore, in the TiO_2-doped samples, surface OH^- groups are resistant to water molecules resulting more stable samples in terms of surface area protection. Furthermore, due to the doping, the M-O-Si (M= Al, Ti) bonds are more polar and stronger than the pure silica case which in turn stabilizes the surface. The comparison of the Al_2O_3 doping on the surface (0.5 %) and into the bulk (1.0 %) of SiO_2 reveals that the former shows an enhanced hydrothermal stability related to the higher concentration of the doping material on the surface.

The results of this study shows that flame hydrolytically synthesized Al_2O_3- and TiO_2-doped silica samples are promising materials not only due to their high purity and also due to their use under harsh hydrothermal conditions of catalysis applications.

ÖZET

İsli metal/metaloit oksitler (örneğin; alümina, titania, silika vb.) kimya endüstrisinden gıda teknolojilerine kadar geniş yelpazede kullanıma sahip önemli hammaddelerdir. İsli silikanın, SiO_2, farmasötik katalizör, petrokimyasal parçalama ve biyolojik atıkların yeniden kazanımları için üretilen katalizörlerin uygulamalarında yaygın kullanılmasından dolayı hidrotermal stabilitesi önemli bir etkendir. İsli silika bazlı malzemelerin; geniş yüzey alanına (50 - 400m^2/g) ve yüksek por hacmine sahip olmaları kataliz uygulamalarında aktif bölgelerin yüzeyde verimli olarak dağılımına ve büyük moleküllerin difüzyonunun kolaylaşmasına imkân vermektedir. Ancak isli silikanın suya karşı düşük stabilitesinden oluşan yüzey hidrolizi, uygulama alanlarını kısıtlamıştır. Bu yüzden stabiliteyi artırmaya yönelik bu alandaki ArGe çalışmaları yüksek ilgi görmektedir. Silikanın hidrotermal stabilitesini artırmak için tuz katkısı, por duvar kalınlıklarının geliştirilmesi ve silikanın üretim süreci sırasında veya sonrasında yapılan hetero atom eklemeleri dahil olmak üzere birçok farklı metotlar kullanılmıştır.

Bu çalışmada, alev hidrolizi yöntemiyle sentezlenmiş isli SiO_2 ve kompozitlerinin hidrotermal stabiliteleri araştırılmıştır. Saf isli silika, isli alümina ve farklı yüzdelerde Al_2O_3 ve TiO_2 katkılı ikili isli karışık oksitler, 24 saat ve 7 gün hidrotermal koşullarda işlem görmüştür. Nitrojen adsorpsiyonu kullanılarak bütün numunelerin yüzey alanları Brunauer-Emmett-Teller (BET) metoduyla, por hacmi ve por maximumları ise Barrett-Joyner-Halenda (BJH) metoduyla hesaplanmıştır. Hidrotermal işlemlemlerin sonucunda, BJH por hacim analizi saf alümina için % 98, saf silika için % 75 ve Al_2O_3 katkılı silica için % 26 düşüş kaydetmiştir. XRD ölçümleri de tüm numunelerin işlem sonrasında amorf yapılarını koruduklarını göstermektedir. BET analizleriyle de hidrotermal uygulamaların, oksitlerin yüzey alanına etkisi ölçülmüştür ve en yüksek fark % 92'lik bir düşüş ile saf alüminanın sonrasında da % 83 ile saf silikanındır. Al_2O_3 ve TiO_2 katkısının SiO_2'nın yüzey dayanıklılığını arttırdığı ve yüzey alanındaki küçülme oranını azalttığı gözlemlenmiştir. Bu iyileştirme, katkı miktarı (% 0.8 – % 1.0) ile de doğru orantılıdır. Örneğin silikaya % 1.0'lık Al_2O_3 veya TiO_2 katıldığında yapının daha stabil olduğu ve (BET) yüzey alanının sırasıyla % 31 ve % 26 azaldığı kaydedilmiştir. Katkı etkisini sıralamak gerekirse eğilim şu şekildedir: TiO_2-katkılı silika > Al_2O_3-katkılı silika > saf silika. Titanyumun alüminyumdan ve silisyumdan daha elektropozitif olması bu sebeple de yüzeydeki -OH gruplarındaki elektronlara olan yüksek ilgisi yukarıdaki eğilimi açıklamaktadır. Aynı sebeple, TiO_2 katkılı numunelerdeki yüzey –OH grupları suya direnç göstererek yüzey alanının daha korunaklı ve stabil olmasını sağlamıştır. Katkı malzemesinin eklenmesi saf silikaya göre

M-O-Si (M = Al, Ti) bağlarını daha da kutuplaştırarak ve güçlendirerek dayanıklı yüzey oluşturur. Silikaya % 0.5'lik yüzey alümina katkısıyla % 1.0'lik yığın katkısı arasında yüzey katkısının daha iyi hidrotermal dayanıklılık gösterdiği görülmüştür, bunun sebebi ise miktarın düşük olmasına rağmen yüzey yoğunluğunun daha yüksek olmasından kaynaklanmaktadır.

Bu çalışma sonucunda hidrolitik alev metoduyla sentezlenen Al_2O_3 ve TiO_2 katkılı SiO_2 ların yüksek saflığı ve sert hidrotermal koşullardaki dayanıklılığı sebebiyle katalitik uygulamalar alanında gelecek vadeden seçenekler arasında olduğu belirlenmiştir.

ACKNOWLEDGEMENTS

I would like to thank the following people for all their support and motivation during my master's and undergraduate studies.

First and foremost, I would like to thank my supervisor Prof. Dr. Mehmet Somer for all his guidance, endless support, and many life lessons. He provided me infinite freedom to conduct my research in his laboratory.

I want to express my sincere thanks to my thesis committee members Assoc. Prof. Dr. Güldem Kartal Şireli and Assoc. Prof. Dr. Uğur Ünal for their precious comments on my research.

I want to thank all my professors and instructors at Koç University. I learnt a lot from them during my master's and undergraduate studies at Koc University. I would like to recognize Assoc. Prof Uğur Ünal, Assoc. Dr. Özgür Birer, Prof. Dr. Ersin Yurtsever, Assoc. Dr. Funda Yağcı Acar, and Dr. Durata Haciu for sharing their scientific knowledge and experience with me.

I was lucky to have Dr. Annamaria Miko as advisor in my first year of Inorganic Research Laboratory. She thought me everything about the principles of research and how to collaborate with other groups. She was like a family to me. In my undergraduate studies I had the opportunity to work with Dr. Selçuk Acar and he taught me how to handle air sensitive chemicals in the glovebox and work with dangerous chemicals without burning down the laboratory. I am very thankful to have the guidance of Assist. Prof. Umut Aydemir at my last year of undergraduate study and later on the final part of my master's thesis defense. By the help of him I had a publication when I was an undergraduate student. I have learnt from him a lot and will continue to do so.

I want to thank all of my group members then and now; Kamil Kiraz, Dr. Özge Balcı, Ceren Zor, Sina Khoshsima, Dr. Ferit Siyahcan, Özge Çoşut, Şeyma Özdemir, Dr. Semih Afyon, Dr. Ali Bateni, Ali Baş, Zeynep Gizem Narin, Meltem İpekçi, Tuğçe Üstün, Yasmin Choaie for collaborative work and unique research environment.

I give big thanks to Dr. Ali Bateni for his help and support on my thesis project since the very beginning. He encouraged and helped me every step so far. He was and will be my big brother. I am grateful to have him in my life.

I would like to express my gratitude to Dr. Peter Höhn. I am very lucky to have the opportunity to work with him at the Max Planck Institute in Dresden/Germany. He taught me how to do a collaborative work and research in an efficient manner. He gave me the chance to conduct my research freely and independently in his laboratories. I am also thankful to Dr. Alim Örmeci, Dr. Cevriye Koz, Dr. Alexander Ovchinnikov, Manisha Patak, and Franziska Jach from MPI for their support and the scientific conversations we had.

I would like to also thank to members of KUYTAM, Dr. Barış Yağcı for XPS analysis and SEM images, Dr. Ceren Yılmaz Akkaya for XRF and XRD measurements, and Dr. Amir Motallebzadeh and Dr. Gülsu Şimşek for BET measurements. I also thank to Cansu Yıldırım for their help to evaluate my results and informative trainings. They thought me how to operate the devices and helped me whenever I need them.

As my friends, many thanks to Kübra Bilici, Özge Akarçay, Fatma Demir Duman and rest of my colleagues at Koç University. As she is like my sister and big support throughout my life, I am and always will be very lucky to have Melike Babucci by my side for every step I take for all these years, at Koç and later on. I know she will be there for me every parts of my life.

Finally I am very lucky by having a lovely family and grateful for their never ending support. I am thankful to my parents, Yücel & Nebil Yahyaoğlu and my lovely sister, Ülkü Yahyaoğlu for being there for me whenever I need them.

This research is supported by Evonik Resource Efficiency GmbH. I thank to Dr. Jutta Zimmermann, Dr. Claus-Peter Drexel, and Dr. Frank Menzel from Evonik Industries AG. for their valuable comments and helps.

This thesis is dedicated to those wonderful people…

TABLE OF CONTENTS

LIST OF TABLES

LIST OF FIGURES

NOMENCLATURE

FMO : Fumed Metal/Metalloid Oxide

HTT : Hydrothermal Treatment

XRF : X-ray Fluorescence

XRD : X-Ray Diffraction

BET : Brunauer-Emmett-Teller

BJH : Barrett-Joyner-Halenda

SEM : Scanning Electron Microscope

DLS : Dynamic Light Scattering

XPS : X-ray Photoelectron Spectroscopy

Chapter 1. Introduction

1.1 Fumed Metal/Metalloid Oxides (FMO)

Fumed metal/metalloid oxides, FMO's, such as titania, alumina, silica etc. are widely used in a wide range of industrial, pharmaceutical applications and in agriculture as individual powder additives or components of composite materials [1-3]. FMO's are used in the adhesives and sealants industry besides coating and ink applications as additives for anti-sag, rheology control, and anti-settling properties and in personal care applications to improve and stabilize suspensions like nail polishes, lip glosses, to modify the skin feel by absorbing excess oil, to improve hair care products in bleaching agents, dyes, hair rinses and styling products, to improve the thermal stability of cosmetics. Antiperspirants also contain FMO as a suspending and anti-agglomeration agent to improve the performance of solid stick and roll-on formulations. Cosmetic powders can be turned out to cream by having stable structure and more formulation flexibility and much higher active concentrations [4].

Dry water is another concept which is water droplets surrounded by fumed silica particles. It contains around 98 % water although it is dry powder. It is mostly used in cosmetics to supply and store water like moisturizing make ups. Besides cosmetics, it can be used as a cooling agent because of high heat absorbing capacity of water. The potential application can be in the gas storage method for dry water in the form of gas hydrates. For example, to store and transport methane gas could be easier with by having hydrate formation. Having methane in dry water could be easier and convenient way to use in vehicles that uses natural gas. For another gas storage alternative, dry water can be used for storage of carbon dioxide to reduce the greenhouse gas in the atmosphere. In general, dry water as dry emulsions could help to store and transport hazardous liquids and other harmful chemicals when they get trapped and encapsulated [4, 5].

FMO materials, mostly SiO_2, Al_2O_3, and TiO_2 are used in catalyst production. These oxides are normally available in the nature. However, oxide materials that contains small amount of impurities can have negative effect on catalyst system. Having high purity of synthetic oxides provides the catalyst system flexibility and reliability because oxide materials as carrier support plays direct role in generating or stabilizing the active sites of catalyst. Synthetic silica and metal oxides, alumina and silica, are widely used as catalyst support in industry. With different production processes, variations in reaction parameters, and after

treatment processes, materials can be modified for different industrial applications such as food, agriculture, coatings, pharmaceuticals, electronics, aerospace etc. in which high purity materials are in need. For the catalysis applications especially fumed silica, AEROSIL® and fumed oxides, AEROXIDE® are useful as carrier support materials because of their high purity, high surface area, and stability [5].

As energy catalysts, gas-to-liquid catalysis is important for the oil refinery process to convert natural gas or gaseous light hydrocarbons into heavier, longer hydrocarbons to obtain gasoline and diesel with syngas process as in the Fischer Tropsch process [6, 7]. The reactions are surface driven, therefore; having large surface area and keeping it constant during the reaction increase the reaction efficiency and reaction rate where the desired properties are matched with fumed metal/metalloid oxides [5].

Automotive emission control catalysts play important role in internally combustion engine vehicles for environmental problems. High surface area, high purity, and high stability of the base materials such as AEROSIL® fumed silica and AEROXIDE® fumed metal oxides are the important key parameters in emission control catalysis. The automotive catalytic converters has a ceramic material that has a dense honeycomb structure with wash coat grains and is coated with catalysts [6]. The wash coat is composed of a complex mixture of fine grained, highly porous inorganic oxides and mixed oxides such as alumina, zirconia, or ceria. Having high porosity and high surface area in the wash coat grains covered with catalysts makes the exhaust gases in connect with a bigger area of catalyst at once. The properties of components affect the stability, therefore performance and efficiency of the catalyst. Fumed metal/metalloid oxides help to increase the efficiency of the catalyst because of their desired properties which are high chemical purity, their particle morphology; aggregates of spherical primary particles with narrow distribution of pore size and high heat resistance enabling high temperature working conditions [5].

Table 1.1 Overview of key properties of synthetic silicas [8]

Property		**Fumed Silica**	**Precipitated Silica**	**Silica Gel**	**Aerogels**
Specific surface area (BET)	m^2/g	50 to 500	30 to 800	250 to 1000	250 to 400
Mean primary particle size	nm	5 to 50	5 to 100	3 to 20	3 to 20
Aggregate or agglomerate size	µm	*	1 to 40	1 to 20	1 to 15
Tamped density	g/l	50 to 250	50 to 500	500 to 1000	50 to 125
Loss on drying	%	≤ 3	3 to 7	3 to 6	3 to 5
Loss on ignition	%	3.5 to 5.5	3 to 7	3 to 15	3 to 5
pH value		3 to 5	3 to 9	3 to 8	2 to 5
Pore diameter	nm	Non-porous	≥ 30	2 to 20	≥ 25
Pore diameter distribution		*	Very broad	Narrow	Narrow
Structure of aggregates and agglomerates		Chain-like, branched, or higher	Structure aggregated, low	High agglomeration, (porous)	Aggl. particles (dist. porous)
Thickening effect		Very distinctive	Present	Present	Present

*Not applicable (strongly dependent on dispersion conditions)

FMO's are also known as pyrogenic metal/metalloid oxides because they are produced in a flame and composed of microscopic spherical droplets of amorphous structured material fused into chain-like, branched, and three dimensional particles. Synthetic silica has different properties with different manufacturing processes. In Table 1.1, physical properties of silica with different production methods are compared and there are clear difference in their BET surface areas, aggregate size and agglomerate size, temped density, loss on drying, and the aggregate structure besides some overlaps in different properties. Precipitated silicas produced in wet chemical processes are ground or spray dried and has low structured aggregates. When they are ground or spray dried, the size and structure of aggregates and agglomerates changes. Primary particles are the smallest components of the fumed oxides and they are not in isolated form. They merge and form an aggregate. An agglomerate is composed of many aggregates. They are held together by weak interactions such as van der Waals forces of hydrogen bonds [8]. Pyrogenically produced silicas are chain like branched aggregates and fluffy powder. They are produced without any grinding and spraying. Wet chemical processed and flame hydrolyzed silicas have the primary particles in aggregate and agglomerate form.

Fumed and precipitated silicas have difference in their loss on drying, loss on ignition, and purity. Precipitated silicas produced from aqueous solution resulting higher content of water, 3 % to 7 %. They include alkali, alkaline earth, and sulfate because of production method of precipitation of sodium silicate and sulfuric acid. Fumed silicas, Aerosil® have less impurities than precipitated silicas. It is made from $SiCl_4$, air, and hydrogen. Final product has hydrochloric acid, HCl with the rate of less than 0.025 % [8].

In reviews and books, the major focus is on the investigations of fumed silica applications rather than other oxides. In commercial applications pure fumed silica or a mixture of silica and alumina is used to synthesize the vinyl acetate monomers. Besides, fumed silica and alumina is used as a support in catalysts with impregnation with Pd/K/Cd, Pd/K/Ba, or Pd/K/Au. In vinyl acetate catalysts, fumed silica and silica/alumina with different shapes is also used**.** In a fixed bed reactors, the hydration of olefins is done by using fumed silica supports as in pellet, bead or spherical form. In the study of the gas phase polymerization of ethane, it is reported that using fumed silica as support promotes the activity of catalysts ten times higher rather than using any other silica supports [9].

1.2 Fumed (Pyrogenic) Silica

Fumed Silica is the first material produced by flame hydrolysis (high-temperature hydrolysis) method which is known as AEROSIL® process and developed by the German chemist Harry Kloepfer at 1943 in order to produce white filler and replace industrial carbon black for the tire industry [9]. With further research and development, AEROSIL®, fumed silica become a part of everyday life and was used in many applications; earthquake-proof foundations for buildings, in silicon sealants for bathtubs, in insulation materials, in food industry, in pharmaceutical industry, in paintings, toners, and coating materials, it makes the application easier by using as additives. An overview of the wide range application of fumed silica, AEROSIL® is shown in Table 1.2.

Commercial fumed silicas have surface area between 50 and 400 m^2/g with a primary particle size of 5 to 50nm as seen in Table1.1. Moreover, their structure are explained as predominantly chain-like, branched structure of aggregates and agglomerates. SiO_4 tetrahedrons in fumed silica are arranged randomly forming amorphous structure and causing the absence of a distinct and well defined x-ray diffraction pattern. It appears as a diffuse amorphous halo which resulted of short range order. For the aggregate and agglomerate size, in technical bulletin it is explained as accurate measurement is not possible because of strong dependency on dispersion conditions.

Table 1.2 An overview of the wide range of applications [8]

Applications	Effect	Examples/industry	
Raw material/educt	• Purity • Reactivity control • Composition	• Fire protection glass • High-strength concrete • Catalysis	• Optical fibers • Pharmaceutical products
Rheological additives	• Anti-sedimentation • Dispersing agents • Thixotropizing • Thickening	• Agrochemicals • Battery gels • Drilling fluids • Injectable screw anchor • Diamond suspension • Sealants	• Adhesives • Cosmetic products • Food • Pharmaceutical Products • Rotor blades for wind power plants • Paint/coatings
Filler Material	• Antiblocking • Low thermal conductivity • Scratch-resistance • Reinforcement	• Sealants • Films • Golf balls • High-quality technical rubber products • Insulation material • Plastic bags	• Coatings • Shoe soles • Silicone • Thermal Insulation • Dental composite fillings • Two-component mortar and concrete
Flow enhancer for powders	• Particle separation	• Agrochemicals • Fire-extinguishing powder • Animal feed • Cosmetics • Plastic granulate	• Grinding additives • Pharmaceutical products • Powder dosage • Powder coating • Toner • Food
Insulation material	• Fineness/pore structure • Low thermal conductivity • Low electrical conductivity	• Cable insulation	• Thermal insulation/ vacuum insulation panels
Porous coating	• Pore formation • Pore structure	• Inkjet paper	• Plaster
Abrasion/abrasion enhancers	• Abrasion	• CMP: chemical- mechanical planarization	• Glass polishing • Metal polishing
Controlling triboelectric properties	• Electrostatic charging	• Powder coating	• Toner

The flame hydrolysis method for production of fumed silica, known as AEROSIL® process (shown in Figure 1.1) is developed by Harry Kloepfer, a chemist working for Evonik Industries AG (Degussa AG). Fumed oxides are produced with flame hydrolysis method where temperature range is 1000 – 2500 °C and reactants are introduced into the flame in gaseous phase. For SiO_2 production, oxygen and hydrogen react with silicontetrachloride, $SiCl_4$. In the flame it is vaporized and mixed with dry air and oxygen by having reactions of oxyhydrogen reaction, where water is formed (1.4), and hydrolysis of $SiCl_4$ with the produced water (1.5).

$$\mathbf{2H_2 + O_2 \rightarrow 2H_2O} \quad \mathbf{(1.1)}$$

$$\mathbf{SiCl_4 + 2H_2O \rightarrow SiO_2 + 4HCl} \quad \mathbf{(1.2)}$$

$$\mathbf{SiCl_4 + 2H_2 + O_2 \rightarrow SiO_2 + 4HCl} \quad \mathbf{(1.3)\ overall\ reactions}$$

In the reaction chamber, gaseous $SiCl_4$ burns in the hydrogen flame. When the water is formed, it reacts with $SiCl_4$ by producing silicon dioxide with only byproduct, hydrochloric acid. After the aerosol, mixture of gases and solids, is cooled down, it is separated into solid and gas parts. Deacidification process is applied to remove HCl gas absorbed on the surface. The reactants used in production are highly volatile compounds obtained from distillation process and highly pure. By changing reaction parameters and conditions in the flame, concentration of the reactants, flame temperature, dwelling time of the gas in the combustion chamber, it is possible to vary the material properties of product such as particle size, particle size distribution, specific surface area, and the surface properties within a broad region [8].

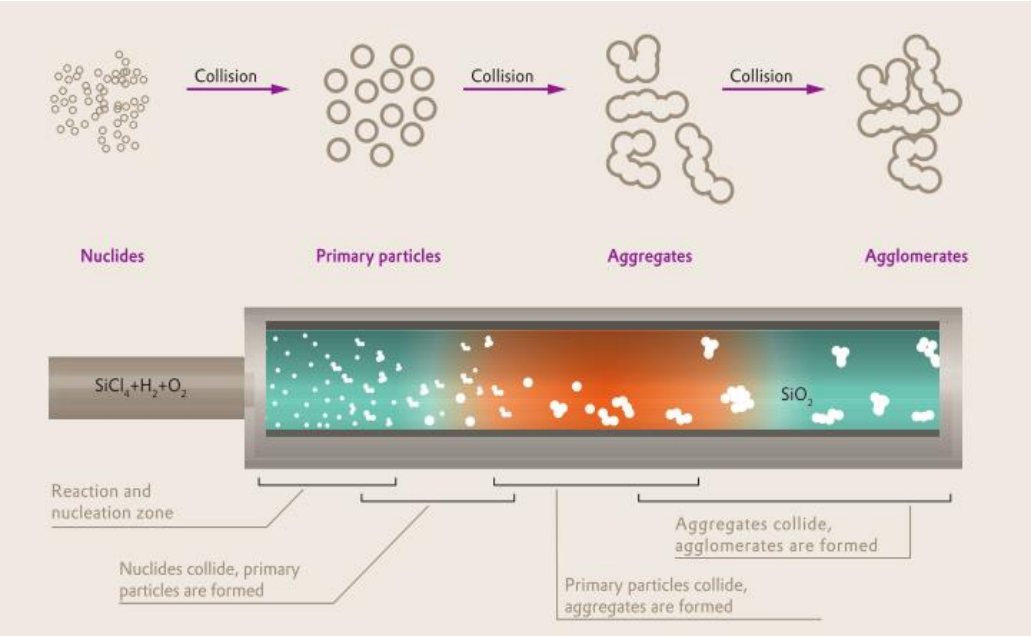

Figure 1.1 Preparation scheme of fumed silica in the flame [8]

The shape and the other properties of flame hydrolyzed product can be explained by droplet model of nucleus. The reaction occurs in a region of with a sharp increase in temperature followed by a decrease in the flame. At the hottest part of the flame, when the reactants meet with flame nuclide droplets of SiO_2 are formed. Formed nuclides collide and merge with each another and get a bigger droplets in liquid phase as long as flame is hot enough. This part is for formation of primary particles. Solidification of the droplets occur when the droplets enter a colder part of the flame. Solidification can be partial. In the colder part, primary particles partially merge and collide resulting aggregates rather than merging fully and having larger spherical droplets. Aggregated structure is formed with coagulation (collision of primary particles) and coalescence (sintering) by forming cluster of primary particles coming together by strong chemical bonds. When they continue to the colder part, they could not merge only can attach to each other by weak interactions forming agglomerates explained as loose accumulations of aggregated particles by having van der Waals forces and hydrogen bonds. The reaction mechanism is illustrated in Figure 1.1. Primary particle size and degree of aggregation and agglomeration depend on flame temperature, hydrogen to oxygen ratio, silicon tetrachloride concentration, residence time in the nucleation zone and aggregation zone in the flame reactor [8].

Besides using silicon tetrachloride for fumed silica synthesis with AEROSIL® process, methyltrichlorosilane (MTCS), trichlorosilane (TCS) and precursors like non chlorides can also be used like octamethyltetrasiloxane (D4) and tetramethoxysilane (TMOS). Besides AEROSIL® by Evonik Industries AG, fumed silica is produced by different companies; CAB-O-SIL® by Cabot, HDK® by Wacker, and REOLOSIL® by Tokuyama.

Other metal/metalloid chlorides can also be used as reactants to produce metal/metalloid oxides with the same AEROSIL® method. The oxides of aluminum and titanium are commercialized and used in many projects. Even though fumed silica produced with AEROSIL® method is amorphous, the oxides of aluminum and titanium are partially in crystalline form [8]. Mixed oxides can also be produced with this method by introducing more than one reactants into the flame, such as $SiCl_4$ and $TiCl_4$ together. Different types of products can be produced by changing reactants and flame parameters. Overall, the flame hydrolyzed process is a flexible procedure for production of fumed oxides from the corresponding chlorides of many elements [8, 9].

For the mixed oxides, if the second educt is introduced in a small quantity, the mostly homogenous particles are produced with the metal ion as second educt distributed in the oxide matrix homogeneously. If the components are introduced with relatively equal quantities. Either homogeneous particles or particles that have regions with different stoichiometry may be formed. Oxide mixtures are different from mixed oxides; Oxide mixtures are oxides producing in separate processes and then physically mixed. Two oxides material do not integrate in the structure. Primary particles and aggregates are composed of only one type of oxide. However, agglomerates can be composed of both oxide types.

There are many variations of silica. After production in the flame if they are not treated, they are hydrophilic because of the silanol groups on the surface of primary particles. If they are post treated by reacting silanol groups with organic groups, they can be hydrophobic. With granulation process without using any binder, they can be more compact snow ball structure with bulk density which is the brand named Aeroperl®. The main aim of the granulation is the enlarge the macro particles results in gravity forces exceeding the van der Waals forces, contributing to better flow properties required for improved processability and accurate dosing. Aeroperl® is the brand name of special granulated fumed metal oxides that helps to handling by reducing dust formation. Aeroperl® is produced from Aerosil® or Aeroxide by having granulation process without using any binders with an average diameter in the range of 20μm to 40μm. With this method Aeroperl®, granulate of pure fumed metal oxides is highly porous and has a bulk density, and flowability by using fixed and fluidized bed reactor. The main characteristics of Aeroperl products are; high temped density, reduced dust formation, optimized flowability (for better handling), high adsorption features, high degree of porosity (meso and macro pores), and well defined particle size distribution.

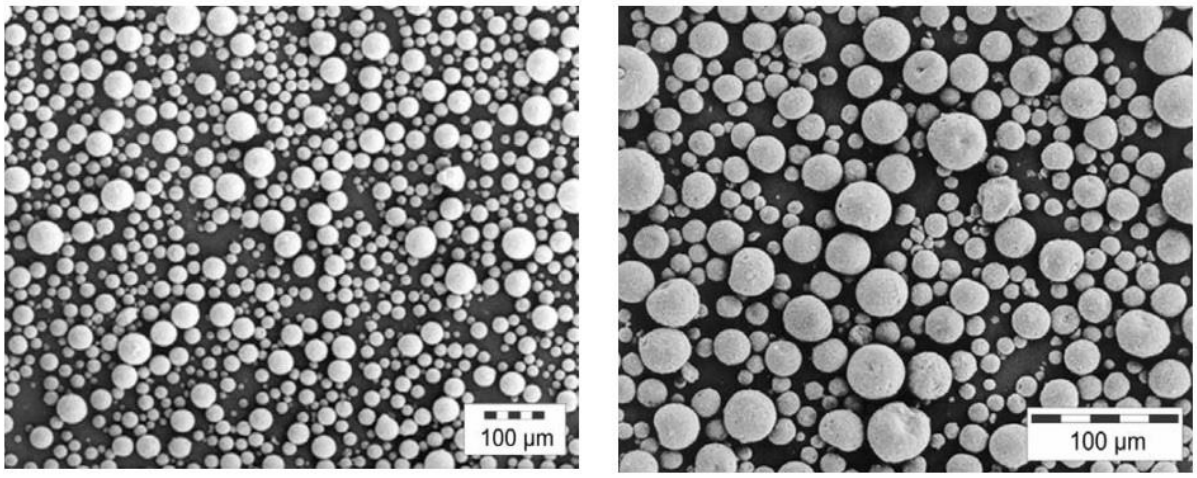

Figure 1.2 Scanning electron microscope images of AEROPERL® Alu 100/30 on the left, and AEROPERL® P25/20 on the right [10]

Unique shape of spherical Aeroperl can be seen in Figure 1.2 showing the SEM image of two different Aeroperl products (on the left alumina based, and the right titania based). Well-formed spherical shape of the Aeroperl particles does not depend on chemical composition. Having macro and mesoporous structure in Aeroperl makes them used as carriers and adsorbents. Figure 1.3 shows the porous surface of silica based Aeroperl with different magnifications.

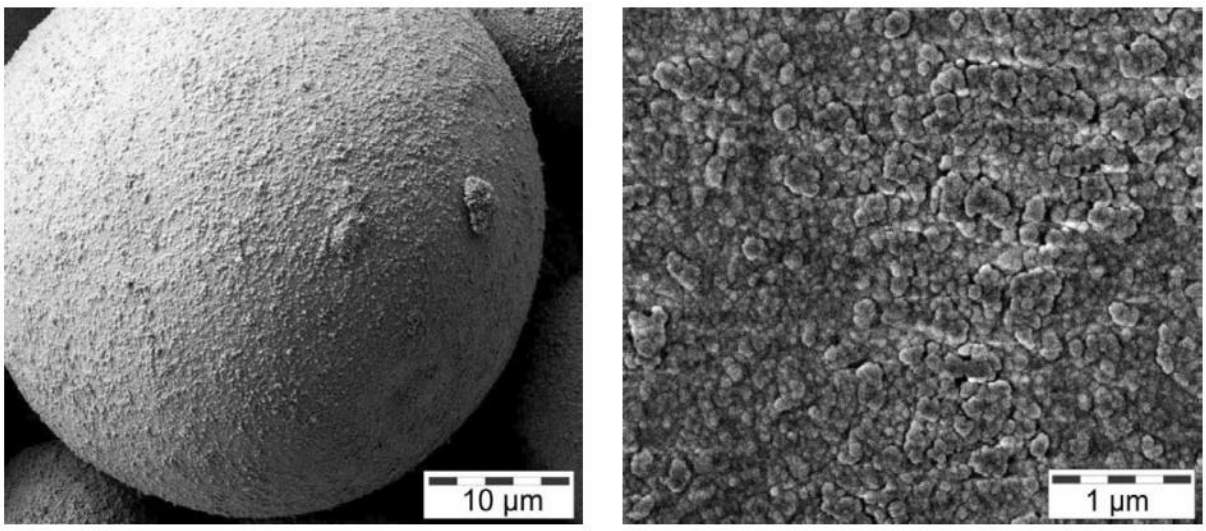

Figure 1.3 Scanning electron microscope images of AEROPERL® 300 Pharma at different magnifications [10]

Having unique particle size distribution and spherical shape of the Aeroperl® makes them show an improved flowability causing easier to handle than Aerosil and Aeroxide products. It is the important parameter for Aeroperl when it is used as carrier. The flowability of Aeroperl does not change even after material is introduced in liquid form. Improved temped density of the Aeroperl makes them have reduced storage space, less dust formation, easier weighing, and faster integration. They granulates 10 to 30 % of the space and this makes the temped density of Aeroperl products 10-times higher when it is compared with Aerosil and Aeroxide products with the same BET specific surface area [10]. Besides positive properties of Aerosil® fumed silica such as high surface area and low metal content (in trace amount), it wets the reaction slurry slowly while increasing the viscosity which is undesirable. Having Aeroperl®, granulate form of Aerosil® wet the slurry more rapidly while not affecting the viscosity [5].

In addition to their comparatively large surface area, well defined spherical primary particles, and high chemical purity, surface chemistry of the fumed silica is another important part for using in various type of applications. The main functional groups on the surface are siloxane (Si-O-Si) and silanol (Si-OH) groups as shown in Figure 1.4.

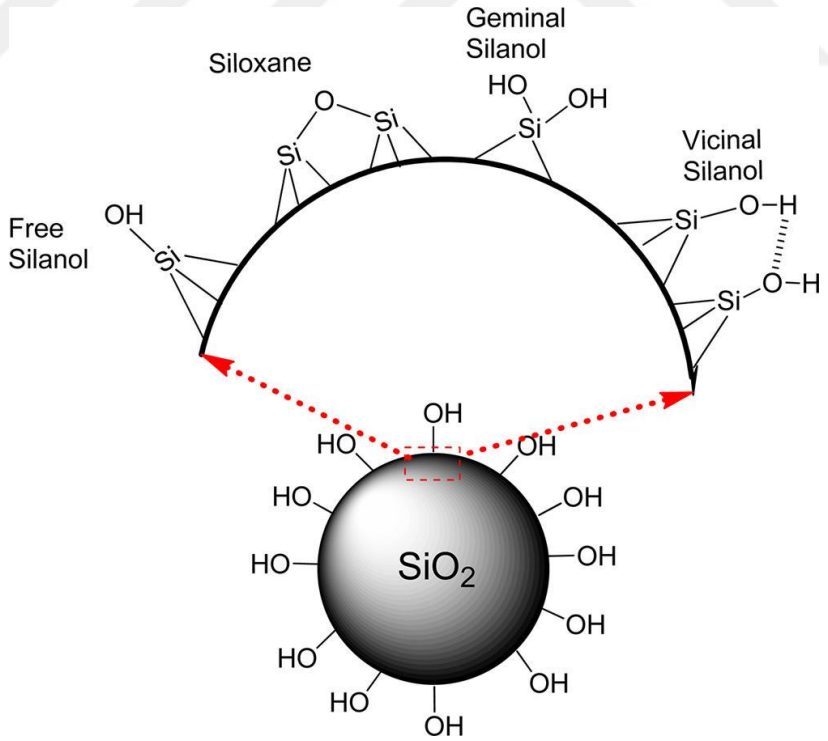

Figure 1.4 Surface functional groups on the silica particles [11]

The silanol groups have hydrophilic nature while the siloxane groups are chemically inactive and have hydrophobic nature. Fumed silica which is not post treated shows hydrophilic nature, because the silanol groups are dominant. To convert them into hydrophobic product, the surface silanol groups are reacted with organic groups. After this procedure, organic group is attached to the surface by covalent bonds. The surface treatments such this application, makes different physical and chemical properties on non-treated fumed silica that helps to widen potential application of fumed oxides [8].

Hydrophilicity of the silica surface determines the surface chemistry and reactivity of silica and it is dependent on synthesis conditions of fumed silica, influence of adsorption of metal ions, chemical modifications, and hydrothermal treatment with the behavior of silicas in aqueous media.

1.3 Hydrothermal Stability of Fumed Silica

Hydrothermal treatment (HTT) technique refers to any heterogeneous reaction in the presence of aqueous solvents under high pressure and high temperature conditions (>1atm, >100°C) in a closed system. Hydrothermal treatment of porous silicas; fumed silica, silica gel, etc., effects and changes the particle morphology, surface area, structure and adsorption properties by the condition of HTT such as temperature, pressure, water-solid concentration ratio, and the medium of HTT; aqueous or steam. The changes in the structure is the result of dissolution-condensation on the surface [12].

HTT of porous silicas increases the average pore size while reduces the specific surface area by reason of deterioration of pore walls as a result of hydrolysis of ≡Si-O-Si≡ bonds depending of silica gel particles and treatment temperature as in stated in previous studies [13-15]. In the case of fumed silica [16], the effect of HTT with the same conditions is different from those with porous silica because of different morphology and pore structure. Effect of HTT on different type of silicas; fumed silica, silica gel, hydrogel, dry/wetted xerogel, and wetted gel in the steam or aqueous media depends on the on the surface morphology of the materials.

Since it is promising material for the medicinal preparation such as wet powders and aqueous suspensions, and most importantly in catalysis applications such as cracking petrochemicals, conversion for production of bio-renewables, hydrothermal stability is a critical requirement of the fumed silica. Because of limited hydrothermal stability of mesoporous material, the development of hydrothermal stable mesoporous materials for catalytic applications has gained interest. Many different methods are used such as adding salt, increasing pore wall thickness, incorporating heteroatoms in situ or by post treatments to improve the hydrothermal stability [17, 18].

In this thesis, the stability of flame hydrolytically synthesized fumed SiO_2, fumed Al_2O_3, and binary fumed mixed oxides; SiO_2/Al_2O_3 and SiO_2/TiO_2 samples with various doping percentages are investigated under hydrothermal conditions treating with high temperature and pressure autoclave.

Chapter 2. Experimental Method

Due to the nano/micro size of the materials that could be harmful for the respiratory system, all sample preparations and experimental parts were done under the hood with safety precautions besides using protective masks and gloves. Experimental works done with high pressure autoclave system and high temperature oven systems were done also in the hoods to prevent any injuries or accidents.

2.1 Materials

All aeroperl pure and mixed oxide samples have high chemical purity which are obtained from Evonik GmbH produced by flame hydrolysis. They have reduced dust formation with high temped density, optimized flowability results in better handling, high degree of porosity with meso and macro pores, superior adsorption properties, and well defined particle size distributions. All the materials used for the tests are hydrophilic materials. They are not chemically treated after production in the flame. The properties of the as received materials are given in the Table2.1**.**

Table 2.1 Properties of all as received samples

Generic Name	Samples	Chemical Composition		Doping Percentage (%)	BET Surface Area (m^2/g)
Vp Aeroperl® 300/30-P	S300	SiO_2	pure samples	-	300
Vp Aeroperl® Alu 100/30	A100	Al_2O_3		-	100
VP AlSi 1	SA52/1.0	SiO_2/Al_2O_3	flame mixed	1.0	52
VP AlSi 2	SA202/0.9			0.9	202
Aeroperl® 3377/20	SA65/0.5		flame doped	0.5	65
VP AlSi 3	SA277/0.1			0.1	277
VP SiTi 4	ST54/1.0	SiO_2/TiO_2	flame mixed	1.0	54
VP SiTi 5	ST196/0.9			0.9	196
VP SiTi 6	ST313/0.8			0.8	313

S300 and A100 are pure samples of fumed silica and fumed alumina respectively. Other seven samples are mixed oxides of silica-alumina and silica-titania produced by flame mixing or flame doping. Contributed alumina or titania is incorporated into silica by introducing the precursors together in the flame process. The samples are named as the composition of the pure material (S for silica, A for alumina) and the composites (SA & ST, alumina and titania incorporated silica respectively) following by their BET surface area and percentage of incorporated material. Production of the two SiO_2/Al_2O_3 samples, SA65/0.5 and SA277/0.1, are different from the binary samples of SiO_2/Al_2O_3 and SiO_2/TiO_2. The minor component of the binary mixed oxides, Al_2O_3 in this case, is directed towards the surface of the primary particle which is believed that this affects the stability of the surface of primary particles due to sintering [5].

2.2 Hydrothermal Ageing Treatment – Autoclave Setup

For the hydrothermal ageing treatments, autoclave setup is used for high temperature (220-250 °C) treatments under autogenous pressure (23-42 bar respectively) for 24 h and 7 days experiments. Hydrothermal ageing test is performed in a Carl Roth high-pressure laboratory autoclave (Model II) with 250 ml 316Ti stainless steel cylinder, which is designed for max. 300 °C / 200 bar working conditions. It has one monometer cap, one valve which is for an external gas inlet and outlet, and an extra opening that is closed with a screw on the cap of the cylinder as shown in Figure 2.1. The sealing of the setup is checked with a test experiment by applying pressured dry air. The sealing of the setup and the monometer are working efficiently. Thermocouple of the system is also tested and it is also working properly.

Added volume of water which is 32 % volume of the closed system is selected based on previous study [19]. In this case, 32 % volume of the stainless steel is filled with 80-82ml distilled water in which both water liquid and vapor present when the system is heated.

In a closed system, based on Antoine equation ($\ln(P) = A - \frac{B}{T+C}$ where P and T are vapor pressure and temperature, respectively. A, B and C are the constants for each specific components) [20] vapor pressure of water changes based on its temperature which is called autogenous pressure. For instance, at 220 °C water vapor pressure would be 23 bar and at 250 °C pressure would be around 42 bar. At high temperatures, even small amount of change in temperature would change the pressure dramatically since they are exponentially related.

2.2.1 First Generation / Simple Autoclave Setup

5 g. of sample is put directly into stainless steel cylinder. 32 % volume of cylinder is filled with distilled water where both liquid and vapor forms coexist at elevated temperatures.

Figure 2.1 Autoclave setup for hydrothermal treatment before modification

During treatment, even though the temperature and pressure tests are fine, the correlation between temperature and the water pressure does not fit to Antoine equation. It might be the isolation problem at high temperatures and some modification needs to be done.

After 4 h, 12 h, and 24 h test treatments, some brown spots are observed on the sample along with color change on the inner surface of autoclave. Observation of brown spots after hydrothermal treatment might either related to impurities in as-received samples or corrosion happening in the autoclave during the treatment. In order to check the source and nature of these spots and color changes, XRF and XRD is used for both untreated and treated samples.

2.2.2 Second Generation / Advanced Autoclave Setup

Since the acidic sample causes the corrosion on 316Ti stainless steel cylinder of the autoclave, a sample holder should be used. Besides having corrosion, putting sample directly into water destroys the physical properties of the sample, such as flowability, particle size, etc. Therefore; by separating the sample from liquid water using Teflon tube, samples have only contact with water vapor. Since there is no problem with thermocouple locating in heating mantle of the autoclave and the monometer, the problem should be the deviation of the temperature on the system. It is devised that to have better and accurate result to measure the temperature, additional thermocouple is needed. Therefore, for the rest of tests an external thermocouple is added into the system from where there is an extra opening closed with a screw on the cap of the cylinder and it is directly in contact with the water medium in the autoclave (see Figure 2.2.).

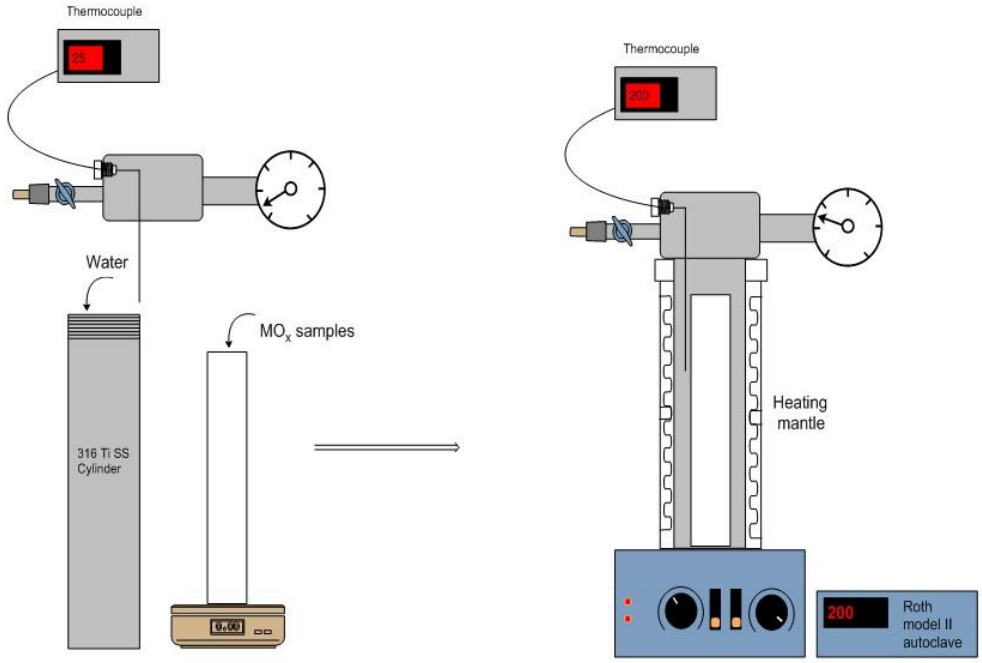

Figure 2.2 Schematic representation of finalized setup for hydrothermal test

After modification of the setup, there are two temperature readings; one from heating mantle and another from the external thermocouple. It is observed that the temperature of the heating mantle is deviated from the temperature of the medium and this difference is higher at elevated temperatures. It is believed that this deviation is originated from the system isolation. In order to solve this problem, setup is isolated with glass wool jackets and some isolators which is shown in Figure 2.3.

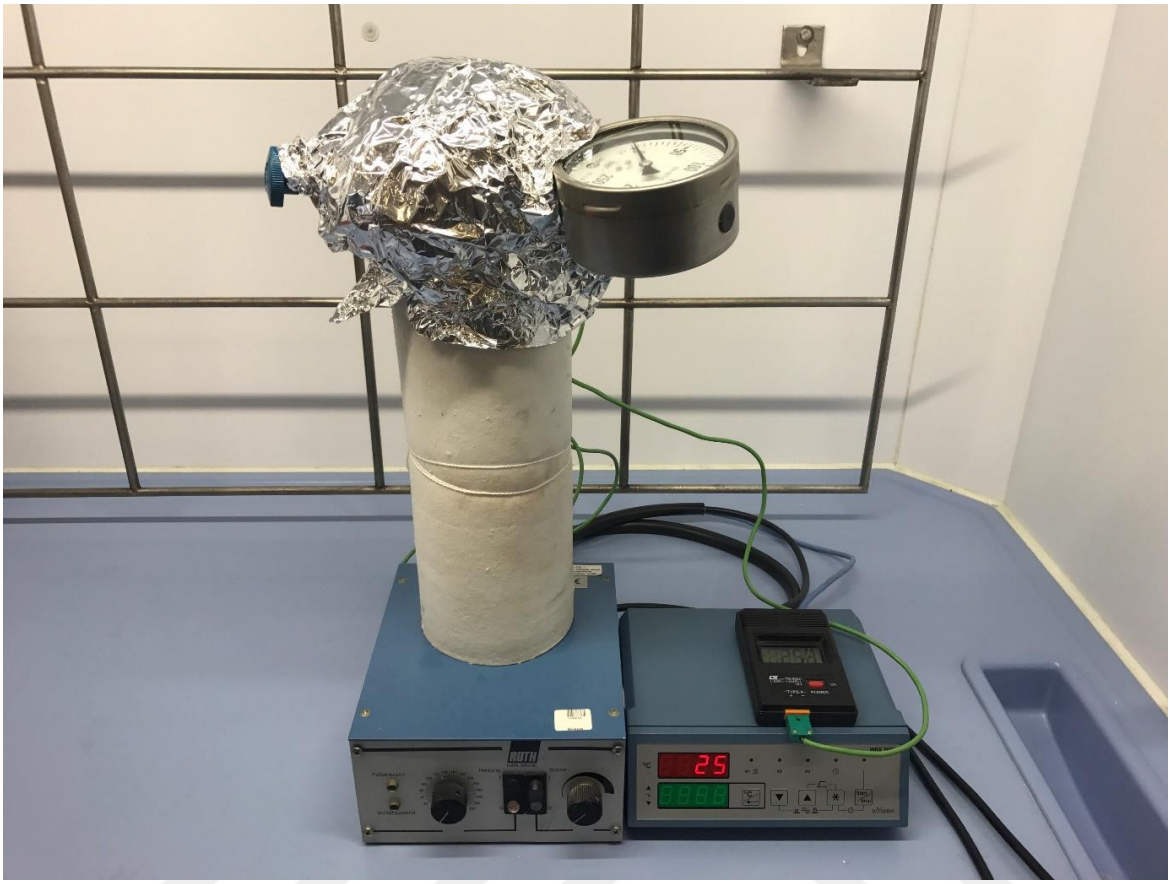

Figure 2.3 Autoclave setup for hydrothermal treatment after modifications

After isolation, pressure – temperature relation based on Antoine equation is satisfied. It should be noted that temperature of the externally added in-situ thermocouple is get as reference where it is directly reading the temperature of the medium.

2.5-3 g. of sample is put into Teflon tube and then placed into stainless steel cylinder which contains 32 % volume distilled water. The samples are treated at 220°C and 250°C for 24h and 7days under autogenous pressure, around 23 and 42 bar respectively.

2.3 Material Characterization Methods and Analysis Theory

2.3.1 X-ray Fluorescence Spectroscopy (XRF)

X-ray Fluorescence (XRF) is an analytical nondestructive method for determination of elemental composition of materials. The method depends on the interaction between X-ray beams produced by a source and electrons of the sample. By absorption of primary beam, the elements in the sample are excited. Then, excited elements emit their own characteristic fluorescence X-rays (fingerprint). XRF is a useful for quantitative determination of all elements except the lightest ones and for qualitative identification of elements with larger atomic number than oxygen [21].

When the sample is radiated by x-rays, an electron from the inner shell of the atom is removed. The vacancy is filled by an outer shell electron by having transition. With transition, x-ray photon is emitted. The difference between two energy levels of electron is equal to the energy of the fluorescent photon which is characteristic of each element. Therefore, the energy of the fluorescent photon gives the information about element and the intensity of it gives the concentration of the element.

There are two types of X-ray Fluorescence instruments, energy dispersive x-ray fluorescence (EDXRF) and wavelength dispersive x-ray fluorescence (WDXRF). The differences of these two devices are x-ray sources, optics, and detectors. In WDXRF there are x-ray monochromator, and a dispersion crystal used for dispersing the fluorescent in the sample and a goniometer to measure the intensity. However, the semiconductor type detector of EDXRF does not need dispersion system with high energy resolution [22].

Elemental analysis of the materials was investigated by using Bruker S8 Tiger XRF Spectrometer with 4KW and Rh anode X-ray tube under Helium atmosphere. Measurements and the calibrations were done by Best Analysis and Elements method. Analysis of the measurements was performed by Spectra-Plus Eval2 V2.2.454.

2.3.2 Powder X-Ray Diffraction (pXRD)

Powder x-ray diffraction (pXRD) method is the most widely used x-ray based analytical techniques among characterization methods which is based on interaction of x-rays and crystalline lattice of sample and used for determination of composition of the material, lattice constants of the unit cell, grain size, and degree of crystallinity in a mixture of crystalline-amorphous substances.

X-rays are generated by a cathode ray tube and filtered to produce monochromatic radiation in order to have a pattern from unique wavelength. Then, collimated beam of x-rays strikes the parallel planes of crystal sample. Each atom of the plane acts as a scattering center and emitted x-rays interfere with each other to produce the diffraction beam, the scattering of a coherent wave by the atoms in a crystal. A diffraction pattern results from interference of the scattered waves and the peaks are observed when the constructive interference satisfy Bragg's Law [23].

Importantly, it can be also used to provide quantitative information of crystalline material beside qualitative information. With p-XRD the percentages of the component of solid mixture can be calculated. X-ray powder diffraction pattern is unique for each crystalline substances. Therefore, chemical identity can be found by matching the patterns from database [24].

2.3.3 Thermal Gravimetric Analysis (TGA)

Thermal Gravimetric Analysis (TGA) is an analytical technique that measures the amount and rate of mass change of the material as a function of temperature or time in a controlled atmosphere. It is a widely used method to characterize the materials and predict the thermal stability by determining the weight loss or gain by reason of decomposition, oxidation or dehydration. The change in the mass of the sample as a function of temperature gives the TGA curve. When the samples are heated, the materials can lose weight because of drying or a chemical reaction by releasing the gas. The samples can gain weight if they react with the gas in the test medium. TGA curve can give the information about purity and composition of the samples, thermal stability, oxidative stability, and moisture content of the samples beside effect of reactive atmosphere medium on the sample [25].

TA Instruments TGA Q500 model instrument is used for the thermal gravimetric analysis of the samples with the temperature range of 25 to 1000 °C and heating rate of 10 °C/min by using a platinum pan in the purge of nitrogen gas. TA Universal Analysis software is used for data analysis.

2.3.4 Brunauer-Emmett-Teller (BET) Surface Area Analysis

Brunauer-Emmett-Teller (BET) analysis provides information about specific surface (m^2/g) area of the materials including pores by physical adsorption of gas molecules on the surface of the solid material and then calculating the amount of gas adsorbed as monomolecular layer. The physical adsorption of the gas results of van der Waals forces between gas and adsorbent surface. Unlikely to chemisorption result in bonding to specific sites on the surface, physical adsorption allows the sorbed molecules to cover all surface and this helps to determination of surface area of the material [26].

Solid materials should be pretreated before performing adsorption. Samples should be de-gased by vacuum, heat or flowing gas to get rid of absorbed contaminants. Then the sample is cooled down to usually cryogenic temperature (77K, -195°C) under vacuum. Adsorbent gas is given to the system with controlled increments. The amount of absorbed gas at each pressure gives the adsorption isotherms. The quantity of gas to form a monolayer physical adsorption is calculated with isotherms to calculate the surface area.

Extending process of monolayer gas adsorption, allowing concentrate the gas in the pores and having adsorption/desorption of isotherms/hysteresis, give the information about the pore structure, size, volume, and area of the sample. The pore sizes and volumes can be calculated from pore size distribution curves after having the adsorption isotherms. The pore size model was developed by Barret, Joyner, and Halenda (BJH) and is applied for calculation of size distribution. The model can be used to determine the pore volume, diameter and distribution [27].

The surface area and the porosity measurements of the samples were done at Analytical Laboratories of Evonik Resource GmbH by the Brunauer-Emmett-Teller (BET) and Barret-Joyner-Halenda (BJH) methods with nitrogen adsorption using TriStar 3000 V6.08 A.

2.3.5 Scanning Electron Microscope (SEM)

Scanning electron microscopy (SEM), is a method for high resolution imaging to determine the surface topography and chemical composition of materials (by having EDX) on a nanometric to micrometric scale. SEM uses high energy electron beams to produce variety of signals by electron-sample interaction to study surface structure [28, 29].

The SEM consists of an electron gun, two condenser lenses, an objective lens, an electron detection system, and a set of detectors, all operating in a high vacuum chamber. In detail, the electron gun (electron source), generates an electron beam which is accelerated down the column. The beam then goes through a succession of apertures which affect various properties of the beam. [29]. In the SEM, the sample under analysis is irradiated with a focused electron beam. The beam can either be probed in a raster-like fashion across the surface of the specimen in sync with a computer display monitor or cathode ray tube to form images or may be fixed to obtain information at that particular position; the voltage used in SEM ranges from 0.1 to 40 kilo electron volts (keV), depending on the material under analysis. The various types of signals produced from the interaction between the primary beam and the sample include secondary electron emission, backscattered electrons, characteristic X-rays, Auger electrons and cathodoluminescence. These signals are gathered from specific emission volumes within the sample and can be used to study several properties of a sample (surface topography, composition etc.) [29].

The most prominent signal produced from the interaction of the primary electron beam and sample is the secondary electron emission signal. A secondary electron signal is initiated when the primary electron beam interacts with an electron from the specimen atom, and loses energy to it; they are characterized by having an energy less than 50 eV [29]. The secondary electron signal is able to resolve surface structures down to the order of 10 nm or better, depending on the magnitude of the primary beam and additional variables (composition of sample etc.). The topographical image produced is dependent on the number of secondary electrons that reach the detector; any SE which do not reach the detector will not contribute the final image, thus, will appear darker in contrast. Mainly, the signal in the SEM is converted to an image made of a series of points called pixels. The intensity of a pixel on the computer screened image represent the intensity of the detected amplified signals. The electron beam moves to next position on the sample and the detected intensity in the next pixel [30]. In this thesis, Zeiss Ultra Plus field emission SEM is used.

2.3.6 Dynamic Light Scattering (DLS) Analysis

Dynamic Light Scattering (DLS) is a technique that measures the size of particles in sub-micron region. With simple DLS measurement at a fixed angle can determine the mean particle size in a limited range. Particles in the solution scatters the light and undergo Brownian motion which is the random movement of particles while solvent molecules surround them. Then, it gives the speed of the Brownian motion with light scattering.

As light scatters from the moving macromolecules, this motion imparts a randomness to the phase of the scattered light and there will be a changing destructive or constructive interference. This leads to time-dependent fluctuations in the intensity of the scattered light. This fluctuations in the scattered light are measured by a fast photon counter. The fluctuations are directly related to the rate of diffusion of the molecule through the solvent, which is related in turn to the particles' hydrodynamic radii. The intensity fluctuations is characterized by computing the intensity correlation function; that provides the diffusion coefficient of the particles. The diffusion coefficient, D is related to the diameter, d of the particles by means of the Stokes-Einstein equation;

$$D = \frac{k_B T}{3\pi\eta d}$$

where k_B is the Boltzmann-Konstant, T the temperature, and η the viscosity.

Since the temperature and the sample viscosity affect the Brownian motion, the parameters need to be known and stable during measurement. The higher the temperature, the more rapid the Brownian motion. The smaller particles are more rapid in Brownian motion whereas the larger ones have the slower Brownian motion.

In this study particle size analysis is performed by using laser diffractometer Malvern Instruments Mastersizer 2000 with Hydro 2000MU adapter with the size range 0.020 – 2000.000 μm.

2.3.7 X-ray Photoelectron Spectroscopy (XPS)

X-ray Photoelectron Spectroscopy (XPS) is an analytical technique that obtain data core electron binding energies of the surface and near surface regions (~10nm) of the materials. The sample is irradiated with low-energy around ~1.5keV X-rays to provoke the photoelectric effect when the binding energy of the electron overcome by the energy of the x-ray photon. Therefore, core level electron is excited and ejected from the surface of the sample. Kinetic energy of the ejected electron is measured by the spectrometer and then the binding energy of the electron is calculated. The photoelectric interaction between surface of the sample and the generated x-rays results in ejection of the electrons which has discrete kinetic energies corresponding discrete electron lines [31].

XPS spectra are obtained with Thermo Scientific K-Alpha spectrometer. Al-K α radiation is used as X-ray source.

Chapter 3. Results and Discussion

3.1 Characterization of Untreated, as Received Samples

The compositions of as received samples were analyzed by XRF spectrometer equipped with X-ray Rh-anode tube. XRF measurements confirm that all samples have high chemical purity as depicted in Table 3.1.

Table 3.1 Elemental analysis of the untreated samples by XRF measurements

Components Formula	**S300** (wt %)	**A100** (wt %)	**SA52/1.0** (wt %)	**SA202/0.9** (wt %)	**SA65/0.5** (wt %)	**SA277/0.1** (wt %)
SiO_2	99.98	-	98.75	99.08	99.48	99.68
Al_2O_3	-	99.98	1.03	0.90	0.50	0.10
Cl	0.02	0.02	0.04	0.02	0.02	0.02

Components Formula	**ST54/1.0** (wt %)	**ST196/0.9** (wt %)	**ST313/0.8** (wt %)
SiO_2	98.96	99.06	99.18
TiO_2	1.02	0.90	0.80
Cl	0.02	0.03	0.02

First two samples, S300 and A100 are pure samples of fumed silica and fumed alumina respectively. The other samples are mixed oxides of silica-alumina and silica-titania which were produced by Evonik Industries via flame mixing or flame doping methods. As explained in experimental section 2.1, the letters and the numbers in the sample name indicate the component of the sample and the surface area of the as received materials. The specimens are named according to the composition of the pure material (S for silica, A for alumina) or the composites (SA & ST, alumina and titania incorporated silica respectively) and by their BET surface area and weight percentage of incorporated material. The synthesis route yields hydrochloric acid (HCl) as byproduct and after deacidification process it remains at a rate of < 0.025 wt %. Therefore; the products are acidic having a pH range of 3.5 - 4.5.

Thermal gravimetric analysis of S300 sample is done in temperature range from 25 to 1000°C with a heating rate of 10 °C/min under nitrogen atmosphere. The Figure 3.1 shows the TGA curve of the as-received silica sample of S300 (pure silica), exhibiting no major mass loss up to 1000 °C. The only mass loss (~ 0.3 %) occurred around up to 200-300 °C results from physisorbed water molecules.

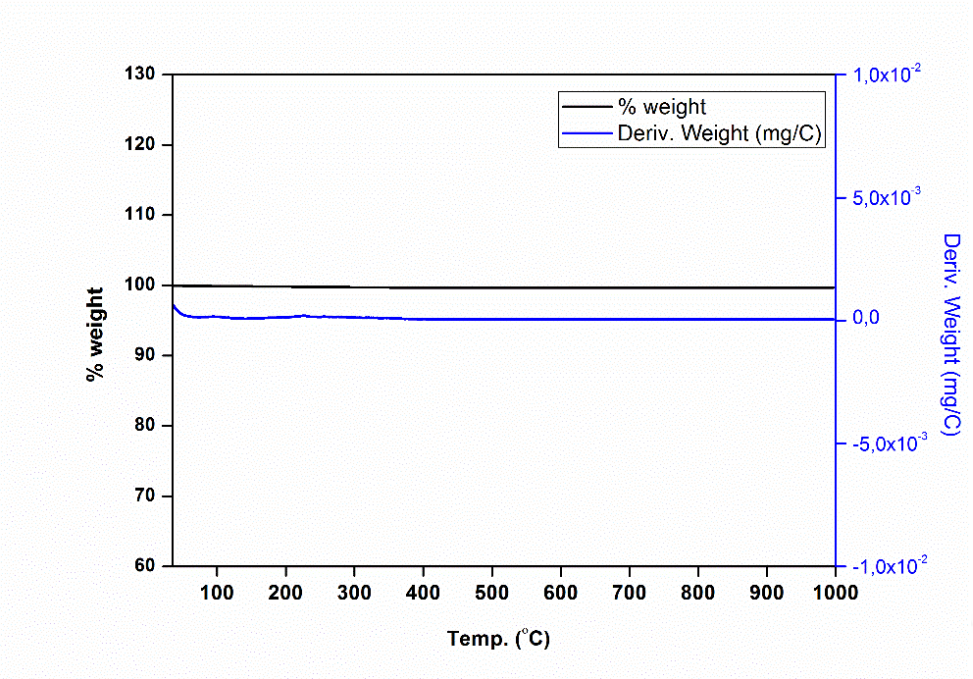

Figure 3.1 Thermal Gravimetric Analysis of S300

3.2 Characterization of Hydrothermally Treated Samples in Simple Setup

On the first series of experiments, a range of initial trials were performed to find optimum reaction conditions. Samples were treated at 200°C for 4, 12, and 24hours without or with external pressure (10-15bar) by adding synthetic air into the system. At the very beginning, samples and water were placed directly into the stainless steel cylinder of the autoclave which resulted in a massive corrosion of the stainless steel container (Figure 2.1). On longer hydrothermal treatments (24h), some brown spots were observed on the sample along with color change on the surface of inner cylinder and formation of residue. In order to investigate the source and nature of these spots and the related color changes, XRF and XRD were used for both untreated and treated samples.

XRF result of untreated and treated samples of SA52/1.0 are shown in Table 3.2. The untreated specimen of SA52/1.0 contains mainly SiO_2 along with Al_2O_3 and trace amounts of Cl. The Cl content in the untreated sample of SA52/0.1 is significant and important when compared with the sample, SA52/0.1 treated at 200°C for 24h using an external 15 bar pressure of dry air. The color shows Fe_2O_3 and Cr_2O_3 contaminations stemming from the 316Ti stainless steel cylinder.

Table 3.2 XRF measurements of untreated and treated samples of SA52/1.0

Components **Formula**	**SA52/1.0** (wt %)	**SA52/1.0 (200°C/24h)** (wt %)
SiO_2	98.75	98.96
Al_2O_3	1.03	0.79
Cl	0.04	-
Fe_2O_3	-	0.10
Cr_2O_3	-	0.01

This finding indicates that presence of Cl in as-received sample is not favorable when stainless steel autoclave setup is employed. Cl is a powerful oxidizing agent and the presence of chloride ion and water is potentially aggressive against stainless steel. It is known that chloride can penetrate the passive layer of stainless and allow corrosion to occur. Based on autocatalytic mechanism pitting corrosion of stainless steel can happen by producing iron hydroxide ($Fe(OH)_2$) with a color indication of brown. $Fe(OH)_2$ is later oxidized to Fe_3O_4 which is thermodynamically more stable [32, 33]. The existence of Fe_3O_4 is confirmed by XRF and XRD analysis which are shown in Table 3.2 and Figure 3.2. Besides, samples treated under aforementioned conditions and directly in contact with water at high temperatures lose some of their critical physical properties, such as flowability, preferred particle size, and surface area. In order to solve the corrosion problem and maintain the physical properties of the specimen, Teflon cylinder was used as a sample holder inside the autoclave.

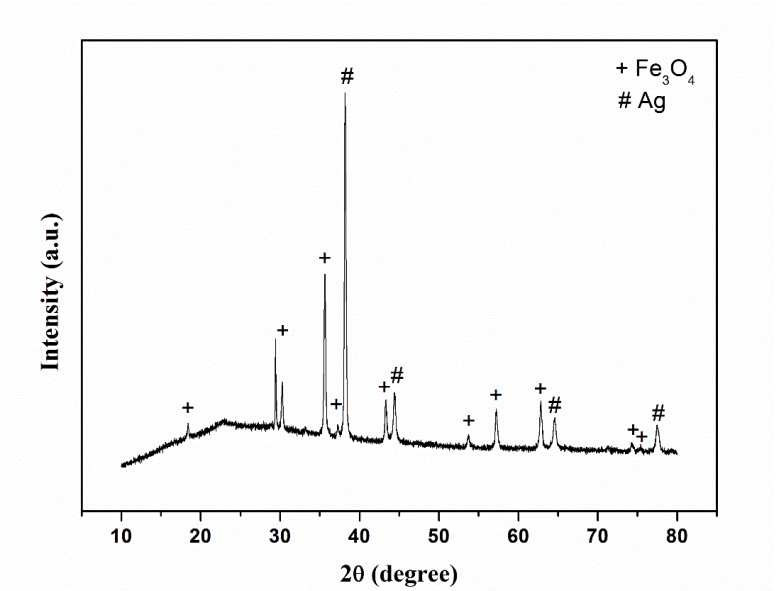

Figure 3.2 pXRD diagram of brown spots as a result of corrosion in stainless steel.

For the test treatments, sample SA52/1.0 was placed into the autoclave for 7 days at 220°C by using Teflon tube without external pressure. After hydrothermal treating again corrosion on the stainless steel was detected as there were some brown particles in the water. Together with silver like particles. Based on the XRF analysis and the XRD pattern of the residue (Figure 3.2), Ag and Fe_3O_4 were the materials which were found in the water outside of Teflon tube. Previously it was mentioned that, Fe_3O_4 forms as a result of corrosion on stainless steel (see Table 3.3) while Ag existence is related to silver joints which have been used in the previous studies. However, we could not find any Ag impurity on the treated samples.

Table 3.3 XRF results of residue particles

Components Formula	**Residue** (wt %)
Fe	51.28
Ag	35.70
Ni	5.14
Cr	2.08
Ca	1.76
Si	1.60
Mn	1.34
Mo	0.55
Mg	0.23
S	0.13
Cl	0.09
Co	0.04
Ti	0.04
K	0.02

3.3 Characterization of Hydrothermally Treated Samples in an Advanced (Final) Setup

In the final setup, a teflon tube is used as sample holder inside the stainless steel cylinder. The added water is placed between the cylinder and teflon tube in such a way only the water vapor is in contact with the sample during the treatment and not with the liquid. Moreover, the thermodynamic correlation between temperature and pressure is achieved by isolating the system after wrapping the autoclave setup with glass wool jacket and aluminum foil. By addition an external in-situ thermocouple, temperature of the water medium in the autoclave could constantly be measured. At working temperatures (220 - 250 °C), even small amount of change in temperature would change the pressure dramatically. When the temperature-pressure correlation and thermal isolation of the system are obtained, the optimum conditions for the hydrothermal treatments are provided.

BET specific surface areas of the samples are determined by nitrogen adsorption method and pore volumes & pore maximums are calculated by BJH method for all untreated and hydrothermally treated samples. Table 3.4 presents the results of hydrothermal treatment of the samples with the treatments at 220 °C and 250 °C for 24 h and 7 days under autogenous pressure, around 23 and 42 bar respectively.

Table 3.4 BET specific surface area, pore volume, and particle size of untreated & treated samples

Samples	Treatment Conditions	BET surface[1] area (m^2/g)	Pore Volume[2] (cm^3/g)	Pore Max[3] (nm)
S300	untreated	300	1.95	38
	220°C/24h	133	1.85	45
	250°C/24h	103	1.47	54
	220°C/7d	65	0.83	72
	250°C/7d	50	0.50	76
A100	untreated	100	1.04	45
	220°C/24h	11	0.05	n.b.[4]
	250°C/24h	10	0.03	n.b.
	220°C/7d	10	0.03	n.b.
	250°C/7d	8	0.02	n.b
SA52/1.0	untreated	52	0.27	75
	220°C/24h	43	0.10	80
	250°C/24h	38	0.10	81
	220°C/7d	38	0.09	84
	250°C/7d	36	0.10	96
SA202/0.9	untreated	202	1.42	38
	220°C/24h	121	1.49	38
	250°C/24h	85	1.40	53
	220°C/7d	79	1.07	56
	250°C/7d	56	0.17	61
SA65/0.5	untreated	65	0.59	40
	220°C/24h	57	0.58	58
	250°C/24h	52	0.59	58
	220°C/7d	49	0.52	78
	250°C/7d	43	0.54	63
SA277/0.1	untreated	277	2.05	45
	220°C/24h	176	2.02	38
	250°C/24h	145	1.97	48
	220°C/7d	116	1.54	49
	250°C/7d	86	0.34	50

ST54/1.0	untreated	54	0.27	60
	220°C/24h	47	0.25	60
	250°C/24h	46	0.20	62
	220°C/7d	41	0.35	57
	250°C/7d	40	0.33	62
ST196/0.9	untreated	196	1.51	45
	220°C/24h	146	0.97	58
	250°C/24h	130	1.24	62
	220°C/7d	131	1.61	79
	250°C/7d	95	0.86	62
ST313/0.8	untreated	313	1.74	33
	220°C/24h	199	1.69	38
	250°C/24h	151	1.77	40
	220°C/7d	148	1.76	67
	250°C/7d	107	1.47	85

[1]Specific Surface Area calculated by the BET method
[2]Mesoporous Volume calculated by the BJH method
[3]Pore Max calculated by the BJH method
[4]Could not be measured

BET surface area for all samples decrease continuously from untreated to 7 days treated samples and this reduction is higher for at 250 °C treated samples in comparison to 220°C. In addition, pore volume also shows a downward trend by increasing treatment temperature while pore maximum shows upward trend In general, the higher the temperature or longer the treatment, the greater are the observed changes in the structural parameters.

The nitrogen adsorption-desorption isotherms of the untreated and treated (250°C/24h, 220°C/7d, 250°C/7d) pure silica, S300 are shown in Figure 3.3. All untreated and treated samples exhibit type IV isotherms with H1 type hysteresis. Having hysteresis in the adsorption-desorption isotherms indicates the presence of mesoporous structure and it appears when the capillary condensation occurs. The effect is representative for all the samples by having the same type of isotherms and hysteresis with the difference of narrower hysteresis and less adsorption.

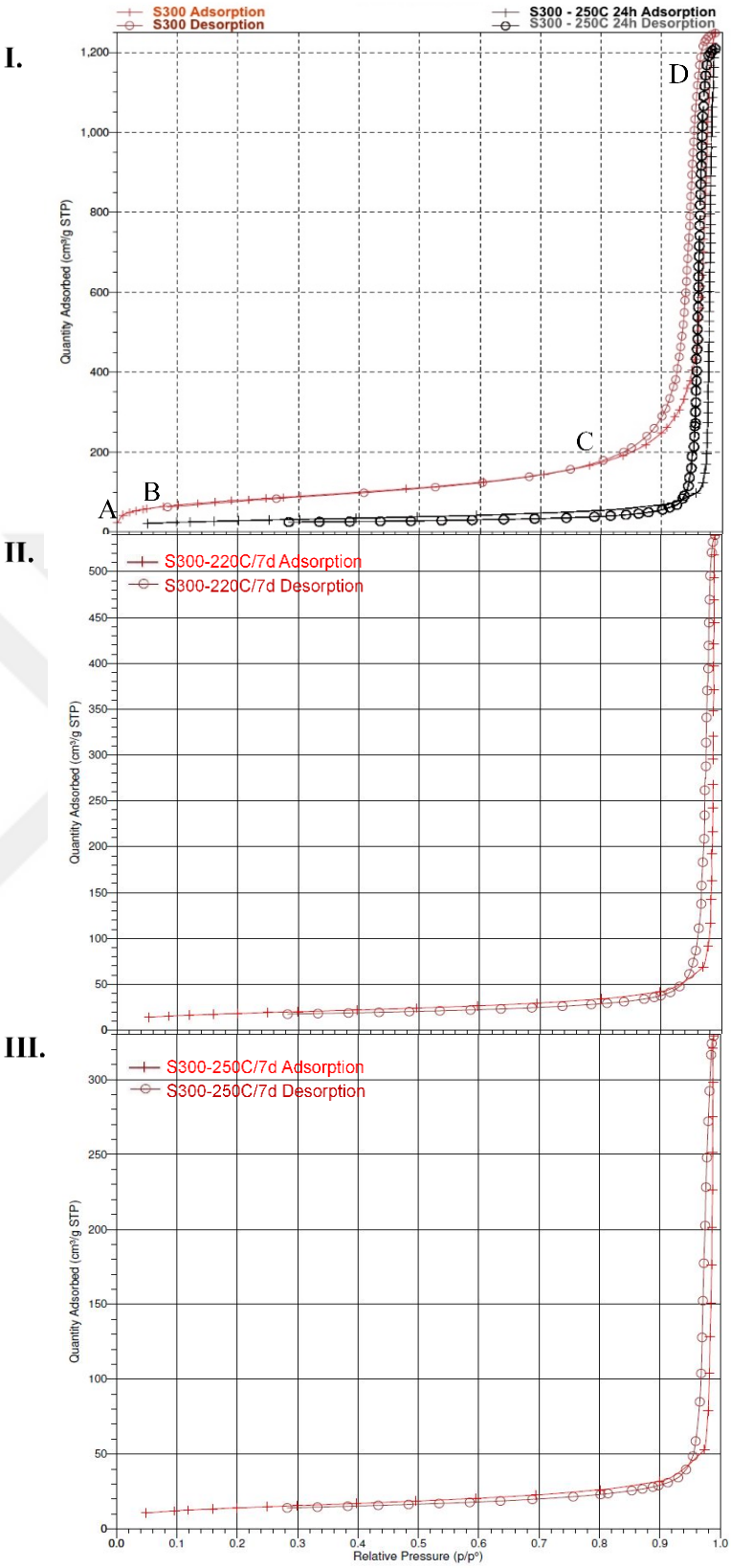

Figure 3.3 Nitrogen adsorption-desorption isotherms of untreated (I. red) and treated (I. black 250°C/24h, II. 220°C/7d, III. 250°C/7d) S300 samples

Initially, at low pressures active adsorption sites, where the pores are less than 2nm, are occupied. Since the adsorption potentials of this microspores are high, it results strong interaction to forces between surface and gas molecules. When the monolayer gas absorption is maintained at (B) as the BET theory explained, the specific surface area is calculated. Along B-C region additional adsorbate layers are formed as the pressure increases. When the large pores, mesopores are filled with condensate because of the capillary forces, saturation point is reached at (D). Later desorption curve displays hysteresis along D-C.

For untreated sample of S300, monolayer adsorption is completed around 100 cm^3/g and the maximum adsorption is above the 1200 cm^3/g. However; for 250°C/24h treated sample (Figure 3.3 I. black) monolayer adsorption is complete about half of the untreated one, around 50 cm^3/g and the maximum adsorption is below 1200 cm^3/g. For one week treated samples at 220 °C and 250 °C (Figure 3.3 II and III.) the monolayer adsorption completions are at around 25 cm^3/g and 10 cm^3/g, with the maximum adsorptions of 550 cm^3/g and 350 cm^3/g. Decrease in monolayer adsorption values are consistent with the decrease in the BET surface area and pore volume data for S300 sample that is listed on Table 3.4 besides the pore volume decreases. The hysteresis loops are getting narrower. The narrower hysteresis loop with decreasing BET surface area explains the some sort of decrease in the porosity of the material. It could be the result of increase in the aggregation of primary particles in secondary particles and the decrease in the size of agglomerates. This effect could be result in the increase in the bulk density [3, 12, 34].

3.3.1 Structural Analysis

Figure 3.4 shows the XRD patterns of untreated and treated S300 (pure fumed SiO_2) and binary sample of SA52/1.0 (1 % Al_2O_3 doped fumed SiO_2).

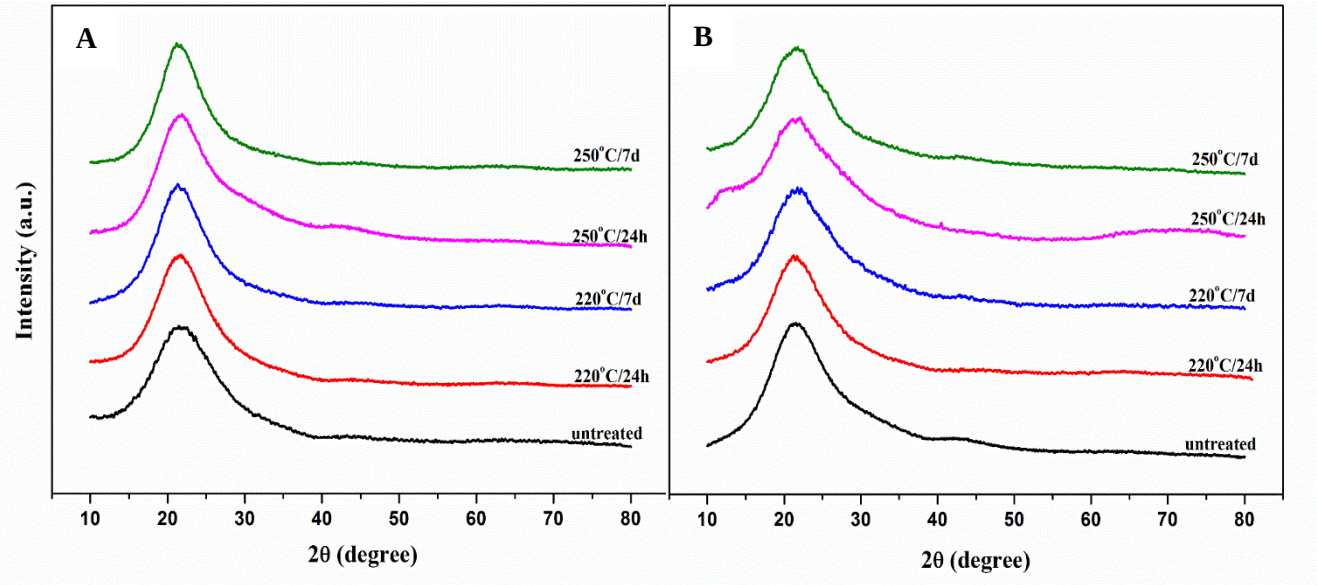

Figure 3.4 pXRD diagram of untreated and treated S300(A) & SA52/1.0(B) samples

Samples are not crystalline and amorphous patterns are observed due to the random arrangements of SiO_4 tetrahedrons in fumed silica. As the samples are treated, amorphous structure of both S300 and SA52/1.0 samples are maintained. Having 1 % of Al_2O_3 does not change the structure after treatment. All other samples with different doping amounts of Al_2O_3 and TiO_2 similar results (please see Appendix, Figure A.1 to Figure A.6), they all have amorphous structures before and after treatment except pure fumed Al_2O_3 (A100).

Fumed alumina, is produced partially in crystalline form unlike fumed silica, Aerosil is amorphous. The crystalline phases are controlled by modifying the process and parameters of production. In the production of flame process, thermal crystallization of Al_2O_3 occurs at lower temperature than the SiO_2. Like A100 sample, it contains δ, γ, and θ alumina phases in varying proportions longer range in such a way the pattern displays combinations of the peaks of alumina phases [8]. As shown in the Figure 3.5, when A100 treated hydrothermally, the structure becomes fully crystalline of aluminum oxihydroxide; AlO(OH), boehmite. Crystallization of A100, fumed alumina can also be explained with BET analysis where surface area is decreased ~ 90 % as shown in Table 3.4.

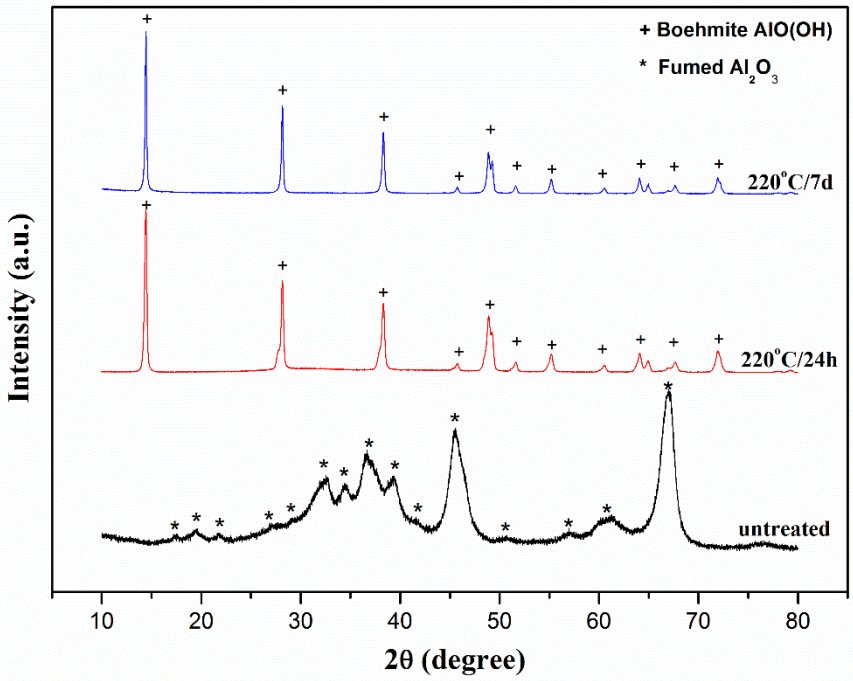

Figure 3.5 pXRD diagram of untreated and treated A100 samples

In Figure 3.6, Figure 3.7, and Figure 3.8 SEM images of the S300, A100, and SA52 samples are displayed at different magnifications respectively. The images on the left (A.) demonstrate the differences in macro morphology of the samples as they are treated (I. untreated, II. 220°C/7d, III. 250°C/7d). All the samples are granulated and agglomerated samples. They all have the spherical macro structures with high porosity and bulk density in order to help for easy handling as mentioned in section 1.2. Images with higher magnifications gives the idea of surface structure of the materials. As the specimens, S300, A100, and SA52 are treated some changes are observed. (the same change with all other samples, please see Appendix for SEM images of SA65/0.5, SA277/0.1, and ST196/0.9, Figure B.1 to Figure B.3). Moreover, changes in the size of the primary constituents are detected with the highest magnification images (C.)

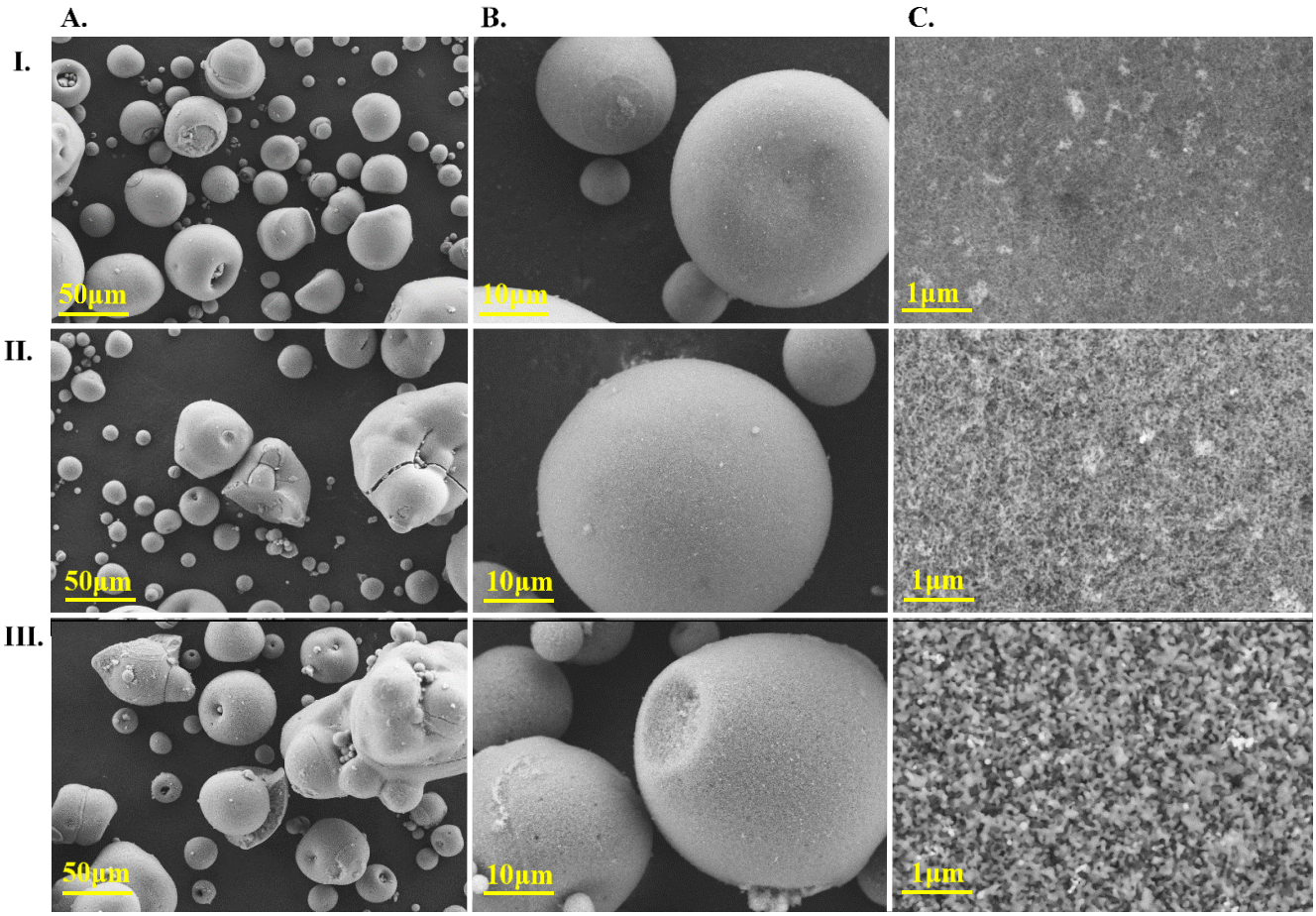

Figure 3.6 SEM images of untreated (I.) and treated (II. 220°C/7d & III. 250°C/7d) S300 samples with different magnifications (A.1.00KX, B.5.00KX, C.50.00KX)

In Figure 3.6, significant changes on the agglomerates and in the size of the primary constituents are observed as the sample (S300) is treated. The specimen could not maintain its spherical structure; particles are collapsed and formed bigger agglomerates beside crushed ones causing smaller ones. After the treatment at 250 °C the changes become more visible and bigger non spherical collapsed particles emerged as was confirmed with the particle size analysis. By employing the highest magnified images (C.), the grains get clearly bigger and become more visible.

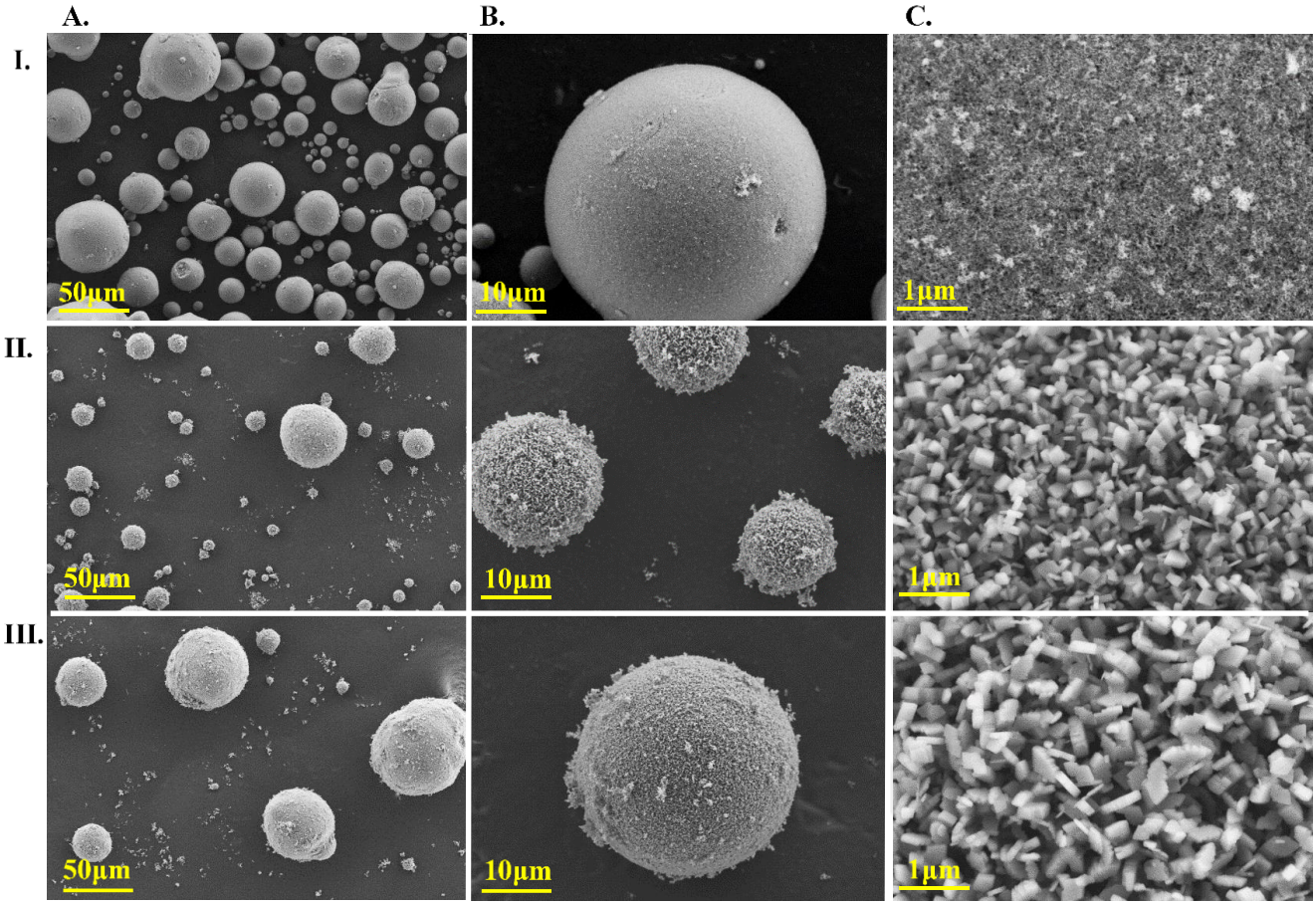

Figure 3.7 SEM images of untreated (I.) and treated (II. 220°C/7d & III. 250°C/7d) A100 samples with different magnifications (A.1.00KX, B.5.00KX, C.50.00KX)

Images of the sample A100 in Figure 3.7, show that untreated smooth spherical particles turn into sphered with rough surfaces with small fragments on each of them. With higher magnification, changes on the primary particles are observed as bigger grains. However, the difference with the previous sample is, A100 that undergoes a phase transformation. As depicted in Figure 3.5, the polycrystalline A100 sample transforms into mono phase boehmite, AlO(OH) which shows that alumina sample A100 is very sensitive to hydrothermal treatment and more unstable compared to silica samples.

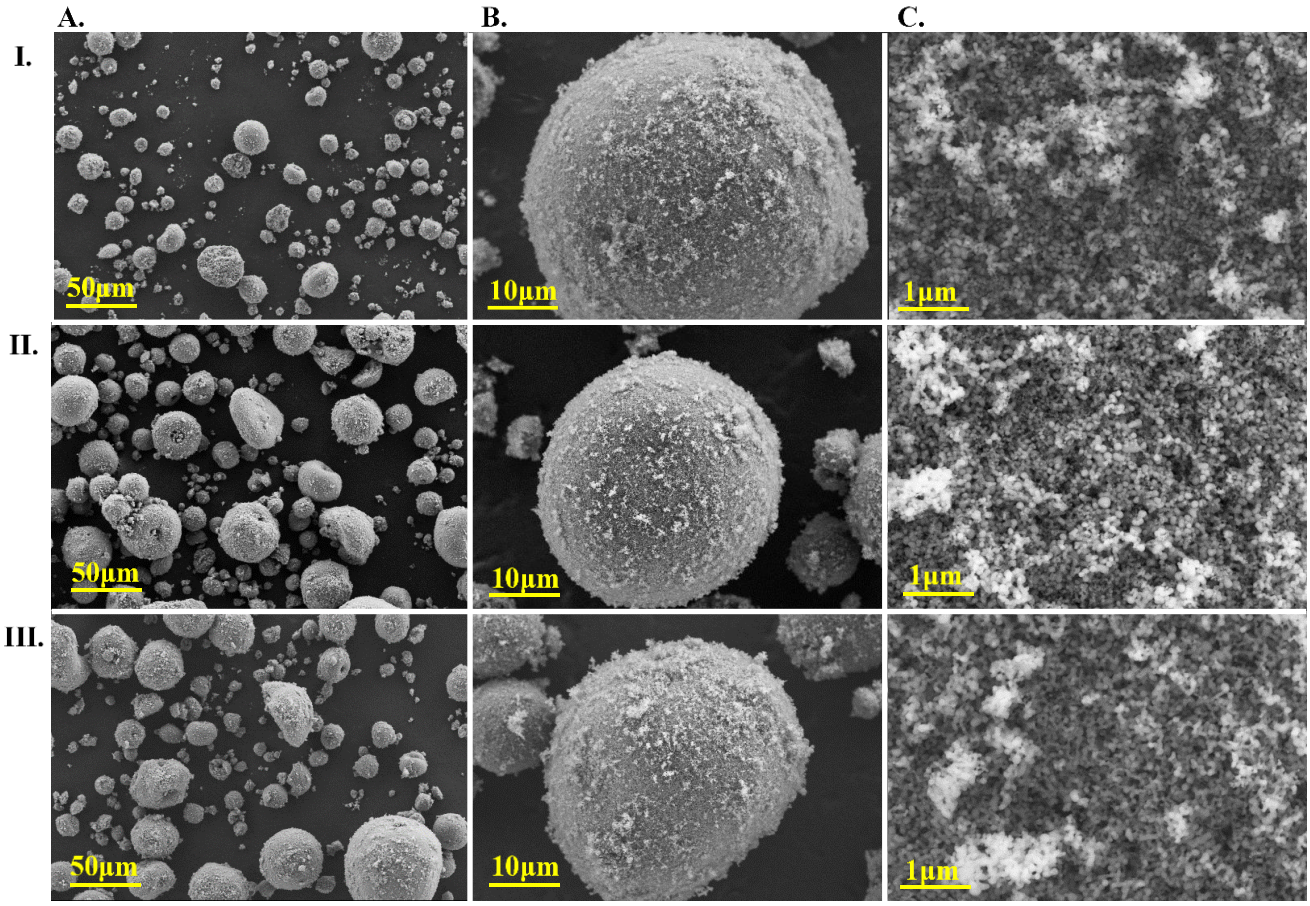

Figure 3.8 SEM images of untreated (I.) and treated (II. 220°C/7d & III. 250°C/7d) SA52/1.0 samples with different magnifications (A.1.00KX, B.5.00KX, C.50.00KX)

Sample SA52/1.0 has approximately half of the size of S300. However, the particle size increases and the shape of the particles become irregular after the treatment (A.). All particles (untreated and treated) have small fragments on the surface. Very likely they stabilize the surface by incorporating aluminum. At the highest magnification, no significant change can be observed in the doped samples after treatment contrast to un-doped S300 and A100 samples after treatment.

In their study of fumed silica under humid conditions B. Morel et al [35] suggest that since there is no shrinkage is observed in the samples, modifications of the contact area between primary silica particles occur during rehydroxylation (Figure 3.9 [35]). Moist atmosphere generates an increase in the contact interfaces area between particles. Since the porosity of the fumed silica is due to the gaps between primary particles in secondary structure, modification leads to a decrease in porosity and BET surface area and also mass transfer from smaller primary particles to larger ones.

The overall process mesopore shrinkage or collapse depends on the chemical reactions that break siloxane (Si-O-Si) bonds. The rate of the process depends on the temperature, pH, and dopant amount.

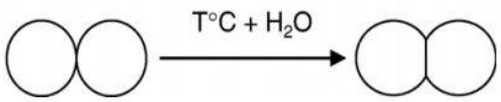

Figure 3.9 Scheme of the evolution of the interface between nano-sized primary particles of fumed silica

Table 3.5 Particle Size Analysis with Dynamic Light Scattering (DLS) Method

Treatment	Particle Size (µm)					
Conditions	**S300**	**A100**	**SA52/1.0**	**SA202/0.9**	**SA65/0.5**	**SA277/0.1**
initial	52.77	39.39	24.46	21.18	67.47	26.97
220°C/24h	53.67	11.18	26.08	24.50	68.24	28.03
250°C/24h	54.47	20.12	29.95	21.77	67.48	28.05
220°C/7d	58.19	21.35	27.46	21.44	67.77	27.28
250°C/7d	52.01	23.55	26.47	22.49	67.50	27.35

Treatment	Particle Size (µm)		
Conditions	**ST54/1.0**	**ST196/0.9**	**ST313/0.8**
initial	23.37	30.84	29.98
220°C/24h	25.93	33.35	30.13
250°C/24h	27.27	32.12	30.79
220°C/7d	26.57	31.96	30.10
250°C/7d	27.91	32.20	30.11

Dynamic Light Scattering method is used for the particle size determination and the results are showing that particle size slightly increases as the samples are treated beside some irregularities. For these materials, agglomerate size can be detected and not the primary particle size. It is known that when fumed silica, AEROSIL®, is dispersed in a liquid, particle size distribution can be unstable and differs to a great extent because of the dispersion conditions. To prevent the further agglomeration in the dispersed liquid, additional dispersion force is applied such as ultrasonic treatment for a short time. It helps to break the larger agglomerates which are formed in liquid, into smaller ones with some aggregates.

However; when the particle size results are compared with the sizes seen on the SEM images, there is some diversity in the results. In Table 3.5 average particle size of the S300, 53µm is twice the size of SA52/1.0 which is 24µm. This effect can be seen with the SEM images on Figure 3.6 and Figure 3.8; however, they have lower particle size values. Within the DLS values, they can be comparable. Since SEM images are more reliable than the results from DLS for determination of particle size particularly for fumed silica, one can say that in general DLS method yields higher values than the actual ones due to the calculation of hydrodynamic radii.

3.3.2 Doping Effect Al_2O_3

When the BET surface area reduction of the samples are compared, the results show that fumed alumina, A100, has the highest reduction by 92 % and fumed silica, S300, has 83 % surface area reduction. Doping of Al_2O_3 (0.9 and 1.0 wt %) into the SiO_2 stabilizes the surface and inhibits the surface area reduction. Since the pXRD data and crystallinity on SEM images of fumed alumina, A100, confirms the phase transformation from polycrystalline fumed alumina to aluminum oxihydroxide; AlO(OH), boehmite. Among all of the treated fumed samples fumed alumina, A100, is the least stable under hydrothermal conditions. Al_2O_3-doped silica sample, SA52/1.0 enhanced the stability by having only 0.1% more alumina than SA202/0.9. Even a small amount of Al_2O_3 doping can influence the surface area reduction in a positive way, therefore hydrothermal stability.

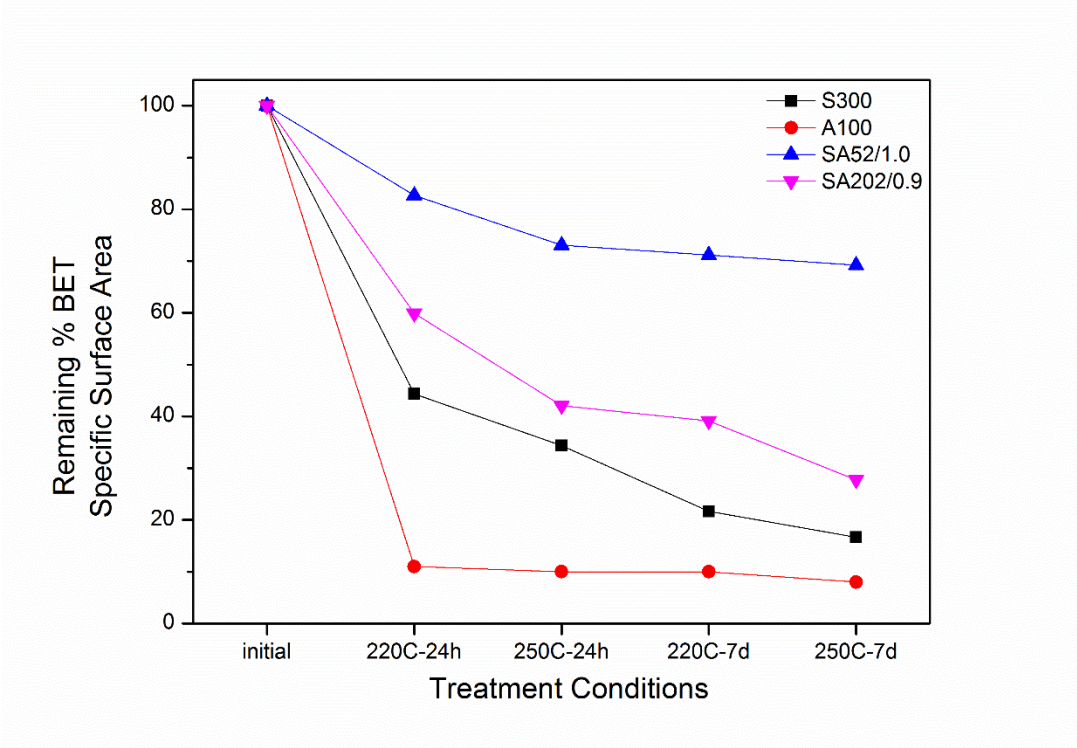

Figure 3.10 BET surface area % change of S300 (pure silica), A100 (pure alumina), and SA52/1.0 & SA202/0.9 (1.0 and 0.9 wt % Al_2O_3 doped) samples for doping effect

3.3.3 Doping Method Effect

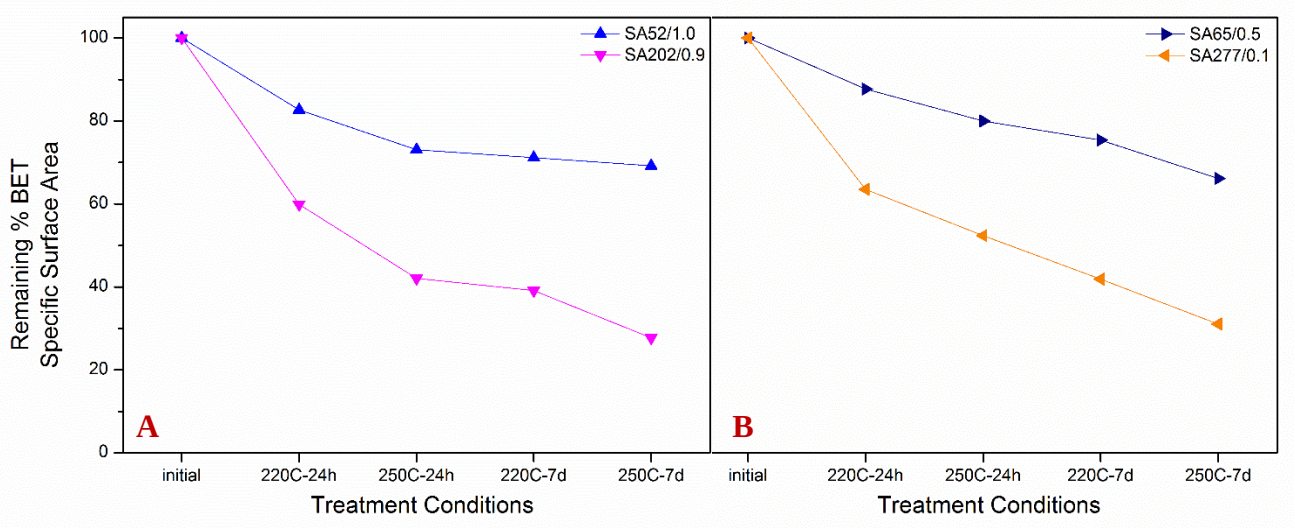

Figure 3.11 BET surface area % change of SA52/1.0 & SA202/0.9 vs SA65/0.5 & SA202/0.9 displaying the influence of doping method

BET results of the samples which are Al_2O_3-doped with different methods are shown in Figure 3.11. By using different procedure in the flame hydrolysis, Al_2O_3 is introduced into bulk SiO_2 (SA52/1.0 and SA202/0.9 in Figure 3.11.A) and on the surface of SiO_2 (SA65/0.5 and SA277/0.1 in Figure 3.11.B). The findings from Fig. 3.11 show that reduction in BET surface area are slightly higher in the SA52/1.0 and SA202/0.9 even though the doping amount of the Al_2O_3 of these samples are much higher than in the SA65/0.5 and SA277/0.1 samples. As it has been reported during the production of these doped fumed silica samples, 1.0 % and 0.9 % of Al_2O_3 is distributed in the whole SiO_2 matrix of SA52/1.0 and SA202/0.9 only small fraction of Al_2O_3 is on the surface of SA52/1.0 and SA202/0.9 compared to SA52/1.0 and SA202/0.9. The location of the dopant-Al_2O_3 in the fumed silica is further investigated through X-ray Photoelectron spectroscopy whose findings are in agreement with the observed BET surface area % reductions. SA52/1.0 and SA65/0.5 samples are investigated by XPS (Figure 3.12) and as expected Al_2O_3 is detected on the surface of SA65 while no signal was obtained for Al_2O_3 on the surface of SA52/1.0 which is obviously below the detection limit.

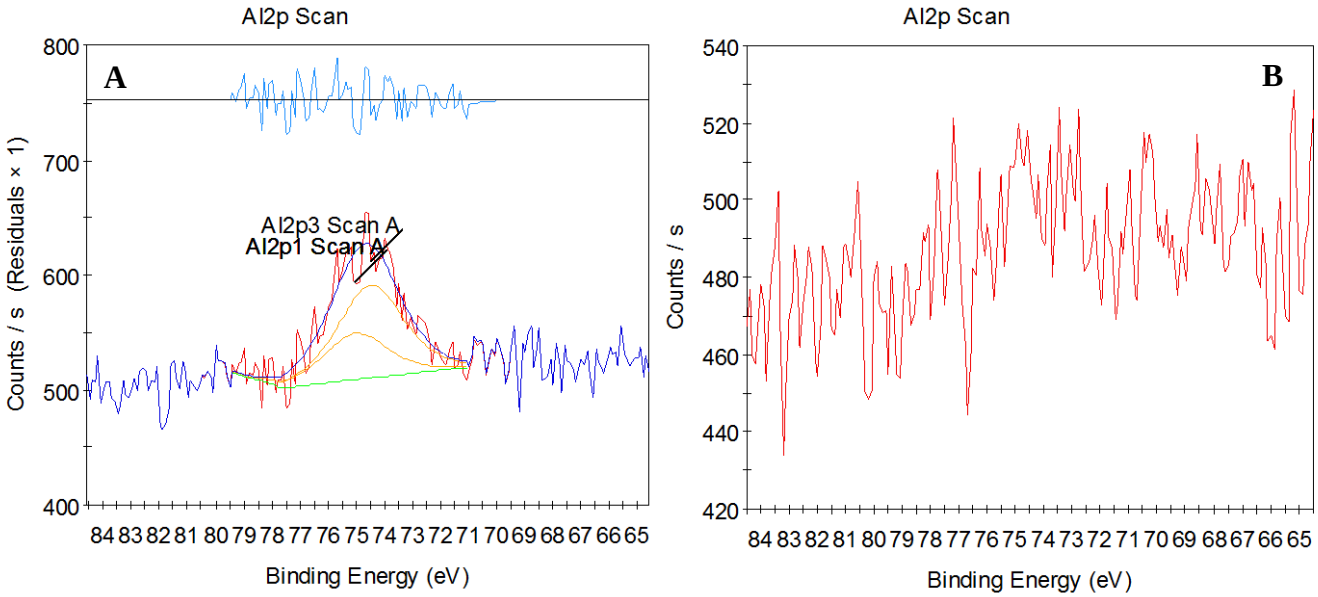

Figure 3.12 XPS results of SA65/0.5 (A) and SA52/1.0 (B)

3.3.4 Doping Effect TiO_2

As shows in Figure 3.11 and Figure 3.13, when the addition of the dopants, Al_2O_3 and TiO_2, dopant increased up to 1.0 %. The decrease of the BET values in the samples become less dominant after hydrothermal treatments.

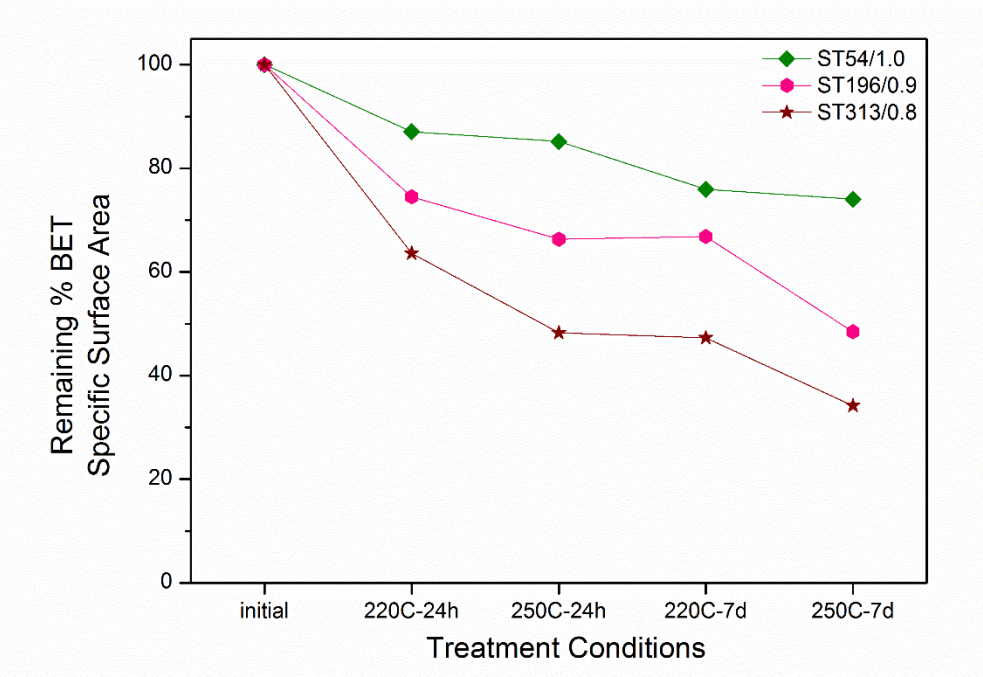

Figure 3.13 BET surface area % change of ST54/1.0, ST196/0.9, and ST313/0.8 for dopant composition effect

3.3.5 Dopant Effect, Al_2O_3 vs TiO_2

When the BET reduction of 1.0 % and 0.9 % Al_2O_3- and TiO_2-doped samples, (SA52/1.0 vs ST54/1.0, SA202/0.9 vs ST196/0.9), are compared as in Figure 3.14, TiO_2-doped samples show better stability than Al_2O_3-doped samples. For 1.0 % doping, BET decreases by 31 % (SA52/1.0) and 26 % (ST54/1.0) and for 0.9 % doped samples by 73 % (SA202/0.9) and 52 % (ST196/0.9), respectively. For both cases, Al_2O_3- and TiO_2-doped samples, the M-O-Si (M = Al, Ti) bonds are more polar and stronger than the pure silica case which in turn stabilizes the surface. Since titanium is more electropositive dopant than aluminum and silicon itself and it has a higher affinity to the electrons of surface OH^- groups. The trend of surface area stabilization by doping follows the order: TiO_2-doped silica > Al_2O_3-doped silica > pure silica.

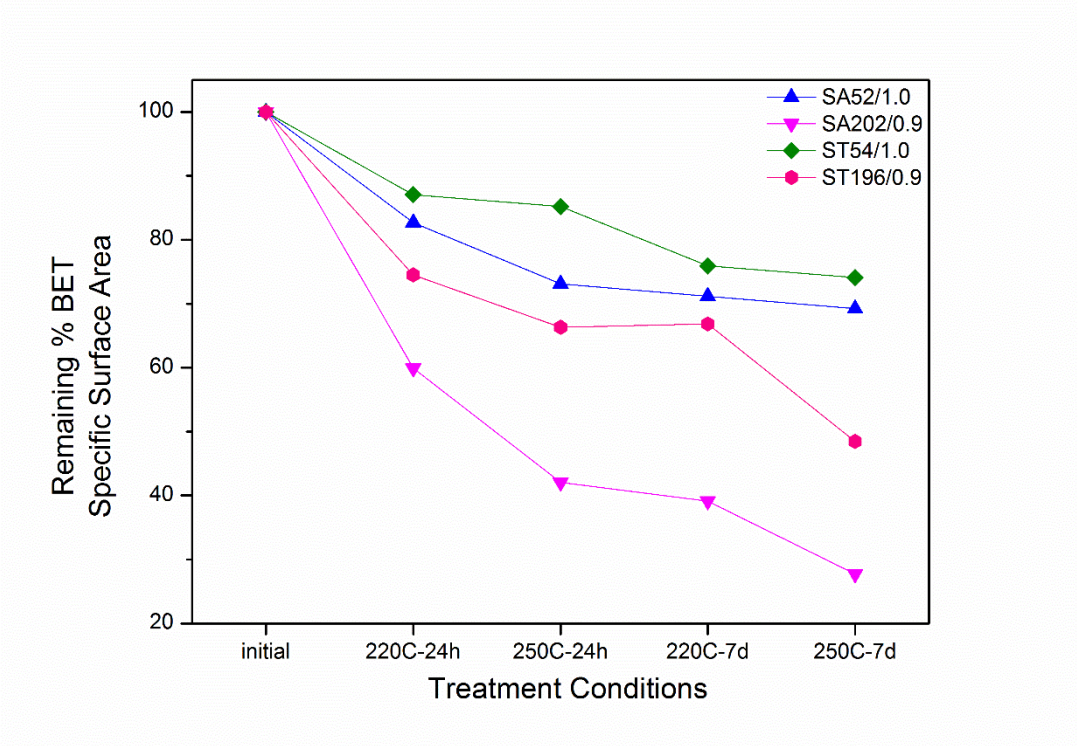

Figure 3.14 BET surface area % change of SA52/1.0 & SA202/0.9 vs. ST54/1.0 & ST196/0.9 to compare dopant effect

According to Yu Han et al. [36] aluminum silicates and titanium silicates which are synthesized as zeolite nanoclusters are more hydrothermally stable than mesoporous pure silica. Introduction of heteroatoms (Al, Ti) in mesoporous material improve the hydrothermal stability. They suggest that having a small amount of extra frame work of Al- and Ti-species can protect the surface of the mesoporous silica from the interaction of water molecule by blocking the surface silanol (terminal OH^-) groups and siloxane (Si-O-Si) bonds resulting enhanced hydrothermal stability. Lutz et al [37] reported that externally introduced aluminum species on the surface makes the zeolites more hydrothermal stable because of forming protective layer against water molecules. Moreover, surface layer of the aluminum rich aluminosilicates act as a protective layer by blocking the silanol groups and siloxane bonds on the surface of zeolites.

The structure and the surface sites of fumed titania and silica/titania are investigated on interaction with water by V. M. Gunko et al [38]. The investigations result that effect of charge distributions for the titania and alumina phases on Si-O(H)-M (M = Ti, Al) and blocking the interaction of the sample with silica with the help of the second phase in agglomerates can cause the stability. Ti-doped samples charges the surface of the materials due to the dissociation of OH^- groups on the bridging Ti-O(H)-Si and it has high polarizability that is higher than that for the Al-doped samples and individual ones. Hydrothermal stability of mesoporous materials by doping metal heteroatoms are investigated by Yin Tang et al [17] and the results are also supporting findings this work. BET surface analysis shows that Co-, Al-, and Co-Al-doping improve the hydrothermal stability of the mesoporous silica, zeolites.

A. K. Datye and coworkers [18] discussed in detail about hydrothermally stable heterogeneous catalysts for conversion of bio renewables. Their result indicates that mixed oxides, especially the amorphous silica–alumina, have better stability than the pure oxides at $T \geq 200°C$ and under superheated system. Results of all these works on hydrothermal stability of mesoporous silica are in line with the finding of this study.

Chapter 4. Conclusion

The stability of flame hydrolytically synthesized fumed silica, fumed alumina, and binary fumed mixed oxides, SiO_2/Al_2O_3 and SiO_2/TiO_2 is investigated under hydrothermal conditions at 220°C and 250°C with autogenous pressure for 24 h and 7 days. X-ray Fluorescence data confirm that all the samples have high chemical purity and the dopant amount of the incorporated amount of Al_2O_3 and TiO_2 in the fumed silica matrix are verified.

Powder X-ray Diffraction analysis revealed that except fumed alumina, all untreated samples are amorphous and they maintain their amorphousness even after the hydrothermal treatment. However; untreated fumed alumina is a mixture of polymorph of δ, γ, and θ alumina phases. After hydrothermal treatment fumed alumina transforms into mono phase of AlO(OH), boehmite.

Scanning electron microscopic (SEM) images show significant micro structural changes in the materials. After hydrothermal treatment particles start to change their smooth spherical form and become rougher on the surface. Particle sizes increase as the particles are collapsed, merged and formed bigger particles. Most notably the primary constituents become larger and more visible. Similar changes are observed on fumed alumina after treatments, where larger particles become apparent as a result of the occurring phase change.

Particle size of the materials are also determined via dynamic light scattering (DLS) generally giving higher values than those obtained from SEM. The reason for this difference is the formation of larger agglomerates in the solution in which the materials are dispersed for the DLS method. Therefore; particle size determination for fumed oxides by using SEM is considered to be more trustable than the DLS method and used for the primary evaluation

Surface area measurements are done by N_2 adsorption-desorption techniques by using Brunauer-Emmett-Teller (BET) analysis method. The results show that fumed alumina has the highest BET reduction by 92 % and fumed silica has 83 % BET reduction. Incorporation of Al_2O_3 and TiO_2 (0.8, 0.9, 1.0 wt %) into the SiO_2 stabilizes the surface and inhibits the surface area reduction. As doping amount increases (0.8 to 1.0 %) surface of the materials becomes more stable.

When the stability of Al_2O_3 incorporated (1.0 %) into the bulk of silica and Al_2O_3 incorporated (0.5 %) on the surface of silica are compared, surface doped samples show enhanced stability and the effect of water molecules on the sample becomes less pronounced. The comparison of percent reduction in BET area of Al_2O_3- and TiO_2-doped silica samples indicates that incorporation of TiO_2 makes the structure more stable to the hydrothermal treatment. Since the electro-positivity of incorporated atoms is higher than silicon, it has the affinity to have electrons of the bonded oxygen of surface OH^- group. Since the electro-positivity of the elements are in the following order: titania > alumina > silica, stability of the materials to hydrothermal treatment is in the following order: TiO_2-doped silica > Al_2O_3-doped silica > pure silica. Moreover, by considering macro structural changes on SEM images and crystallinity beside 92 % BET reduction, fumed alumina is less stable than fumed silica and binary fumed oxides of SiO_2/Al_2O_3 and SiO_2/TiO_2 by hydrothermal treatment.

The results of this work show that flame hydrolytically synthesized Al_2O_3- and TiO_2-doped silica samples are more stable than pure fumed alumina and silica. Therefore, they are expected to be promising materials various uses such as wet powders and aqueous suspensions, and most importantly in catalysis applications as wells as cracking petrochemicals, conversion for production of bio-renewables because of high chemical purity and stability to hydrothermal conditions.

Bibliography

[1] W. Roberts and H. Bergna, "Colloidal silica: fundamentals and applications," *CRC Taylor and Francis, Boca Raton*, 2006.

[2] V. Gun'ko, V. Zarko, O. Goncharuk, A. Matkovsky, O. Remez, J. Skubiszewska-Zięba, *et al.*, "Nature and morphology of fumed oxides and features of interfacial phenomena," *Applied Surface Science*, vol. 366, pp. 410-423, 2016.

[3] E. Industries, "Basic characteristics of AEROSIL fumed silica," *Technical Bulletin Fine Particles*, vol. 11, 2006.

[4] E. Industries, "AEROSIL ® and SIPERNAT ® Silica : Versatile Raw Materials for Personal Care Formulations Technical Information," *Technical Information* vol. 1251, 2012.

[5] E. Industries, "Inorganic Materials for Catalyst Innovation AEROSIL®, AEROXIDE® and SIPERNAT® Metal Oxides and Silica Based Materials," *Industry Information* vol. 2242, 2011.

[6] A. Dalai and B. Davis, "Fischer–Tropsch synthesis: a review of water effects on the performances of unsupported and supported Co catalysts," *Applied Catalysis A: General*, vol. 348, pp. 1-15, 2008.

[7] F. Morales, D. Grandjean, A. Mens, F. M. De Groot, and B. M. Weckhuysen, "X-ray Absorption Spectroscopy of Mn/Co/TiO2 Fischer− Tropsch Catalysts: Relationships between Preparation Method, Molecular Structure, and Catalyst Performance," *The Journal of Physical Chemistry B*, vol. 110, pp. 8626-8639, 2006.

[8] E. Industries, "AEROSIL Fumed-Silica," *Technical Overview*, 2015.

[9] J. Regalbuto, *Catalyst preparation: science and engineering*: CRC Press, 2016.

[10] E. Industries, "AEROPERL® Granulated fumed oxides," *Technical Overview*, vol. 1341, 2013.

[11] S. Cerveny, G. A. Schwartz, J. Otegui, J. Colmenero, J. Loichen, and S. Westermann, "Dielectric study of hydration water in silica nanoparticles," *The Journal of Physical Chemistry C*, vol. 116, pp. 24340-24349, 2012.

[12] V. Gun'ko, J. Skubiszewska-Zięba, R. Leboda, K. Khomenko, O. Kazakova, M. Povazhnyak, *et al.*, "Influence of morphology and composition of fumed oxides on changes in their structural and adsorptive characteristics on hydrothermal treatment in steam phase at different temperatures," *Journal of colloid and interface science*, vol. 269, pp. 403-424, 2004.

[13] R. Iler, "RK Iler The Chemistry of Silica," ed: Wiley, New York, 1979.

[14] R. Leboda, E. Mendyk, A. Gierak, and V. Tertykh, "Hydrothermal modification of silica gels (xerogels) 1. Effect of treatment temperature on their porous structure," *Colloids and Surfaces A: Physicochemical and Engineering Aspects*, vol. 105, pp. 181-189, 1995.

[15] R. Leboda, E. Mendyk, A. Gierak, and V. Tertykh, "Hydrothermal modification of silica gels (xerogels) 2. Effect of the duration of treatment on their porous structure," *Colloids and Surfaces A: Physicochemical and Engineering Aspects*, vol. 105, pp. 191-197, 1995.

[16] R. Leboda, V. Tertykh, V. Sidorchuk, and J. Skubiszewska-Zięba, "Peculiarities of steam-phase hydrothermal modification of pyrogenic silicium dioxide," *Colloids and Surfaces A: Physicochemical and Engineering Aspects*, vol. 135, pp. 253-265, 1998.

[17] Y. Tang, Y. Chen, Y. Wu, M. Zheng, C. Zhang, M. Yang, *et al.*, "Production of mesoporous materials with high hydrothermal stability by doping metal heteroatoms," *Microporous and Mesoporous Materials,* vol. 224, pp. 420-425, 2016.
[18] H. Xiong, H. N. Pham, and A. K. Datye, "Hydrothermally stable heterogeneous catalysts for conversion of biorenewables," *Green Chemistry,* vol. 16, pp. 4627-4643, 2014.
[19] R. A. Laudise, "Hydrothermal synthesis of crystals," *Chemical & Engineering News,* vol. 65, pp. 30-&, 1987.
[20] C. Antoine, "Vapor pressures: new relationship between vapor pressure and temperature," in *Records of meetings of the Academy of Sciences*, 1888, p. 778780.
[21] D. A. Skoog, F. J. Holler, and S. R. Crouch, *Instrumental analysis*: Cengage Learning India, 2007.
[22] R. Jenkins, "X-Ray Techniques: Overview," *Encyclopedia of analytical chemistry,* 2000.
[23] W. N. Sharpe, *Springer handbook of experimental solid mechanics*: Springer Science & Business Media, 2008.
[24] R. Jenkins, R. Snyder, and R. Cernik, "X-ray Powder Diffractometry, Introduction," *Angewandte Chemie-English Edition,* vol. 36, pp. 1128-1128, 1997.
[25] M. E. Brown, *Introduction to thermal analysis: techniques and applications* vol. 1: Springer Science & Business Media, 2001.
[26] S. Brunauer, P. H. Emmett, and E. Teller, "Adsorption of gases in multimolecular layers," *Journal of the American chemical society,* vol. 60, pp. 309-319, 1938.
[27] E. P. Barrett, L. G. Joyner, and P. P. Halenda, "The determination of pore volume and area distributions in porous substances. I. Computations from nitrogen isotherms," *Journal of the American Chemical society,* vol. 73, pp. 373-380, 1951.
[28] D. C. Bell and N. Erdman, *Low voltage electron microscopy: principles and applications*: John Wiley & Sons, 2012.
[29] J. Goldstein, D. E. Newbury, P. Echlin, D. C. Joy, A. D. Romig Jr, C. E. Lyman, *et al.*, *Scanning electron microscopy and X-ray microanalysis: a text for biologists, materials scientists, and geologists*: Springer Science & Business Media, 2012.
[30] E. A. Varella, *Conservation Science for the Cultural Heritage: Applications of Instrumental Analysis* vol. 79: Springer Science & Business Media, 2012.
[31] J. M. Hollander and W. L. Jolly, "X-ray photoelectron spectroscopy," *Accounts of chemical research,* vol. 3, pp. 193-200, 1970.
[32] R. E. Avery and S. Lamb, "Effect of Chlorine on Common Materials in Fresh Water," 1998.
[33] F.-Y. Ma, *Corrosive effects of chlorides on metals*: INTECH Open Access Publisher, 2012.
[34] V. Gun'Ko, I. Mironyuk, V. Zarko, E. Voronin, V. Turov, E. Pakhlov, *et al.*, "Morphology and surface properties of fumed silicas," *Journal of colloid and interface science,* vol. 289, pp. 427-445, 2005.
[35] B. Morel, L. Autissier, D. Autissier, D. Lemordant, B. Yrieix, and D. Quenard, "Pyrogenic silica ageing under humid atmosphere," *Powder Technology,* vol. 190, pp. 225-229, 2009.
[36] Y. Han, N. Li, L. Zhao, D. Li, X. Xu, S. Wu, *et al.*, "Understanding of the high hydrothermal stability of the mesoporous materials prepared by the assembly of triblock copolymer with preformed zeolite precursors in acidic media," *The Journal of Physical Chemistry B,* vol. 107, pp. 7551-7556, 2003.

[37] W. Lutz, W. Gessner, R. Bertram, I. Pitsch, and R. Fricke, "Hydrothermally resistant high-silica Y zeolites stabilized by covering with non-framework aluminum species," *Microporous materials,* vol. 12, pp. 131-139, 1997.

[38] V. Gun'ko, V. Zarko, E. Chibowski, V. Dudnik, R. Leboda, and V. Zaets, "Structure of fumed titania and silica/titania and influence of the nature of surface sites on interaction with water," *Journal of colloid and interface science,* vol. 188, pp. 39-57, 1997.

Appendix

A. XRD Patterns of the Samples

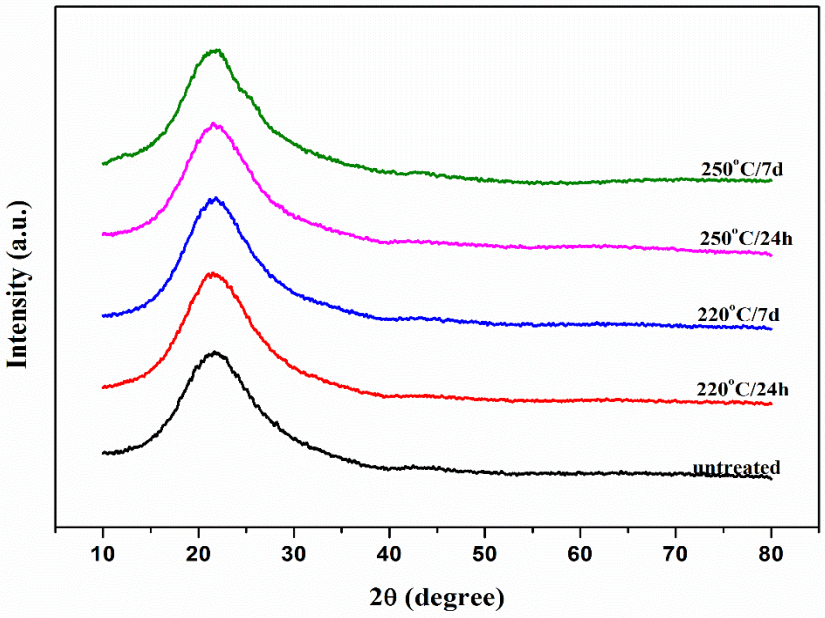

Figure A.1 pXRD diagram of untreated and treated SA202/0.9 samples

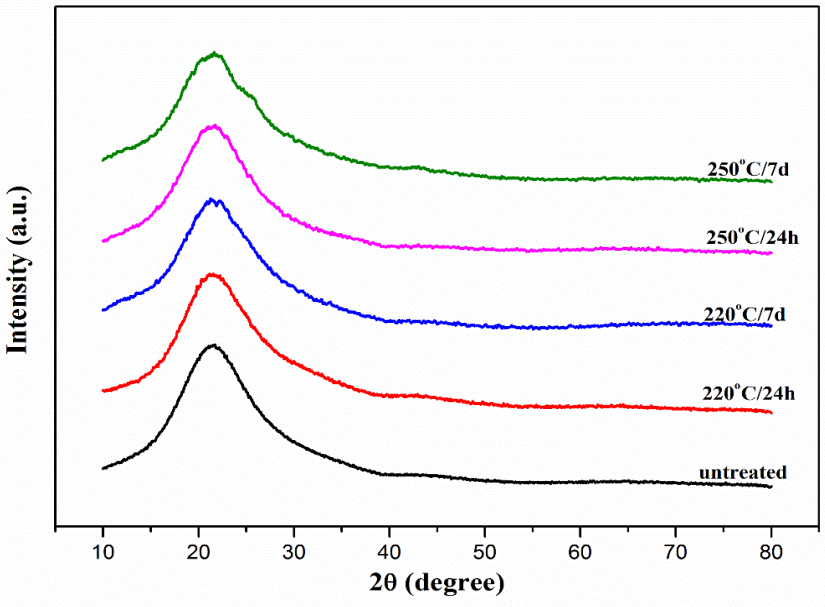

Figure A.2 pXRD diagram of untreated and treated SA65/0.5 samples

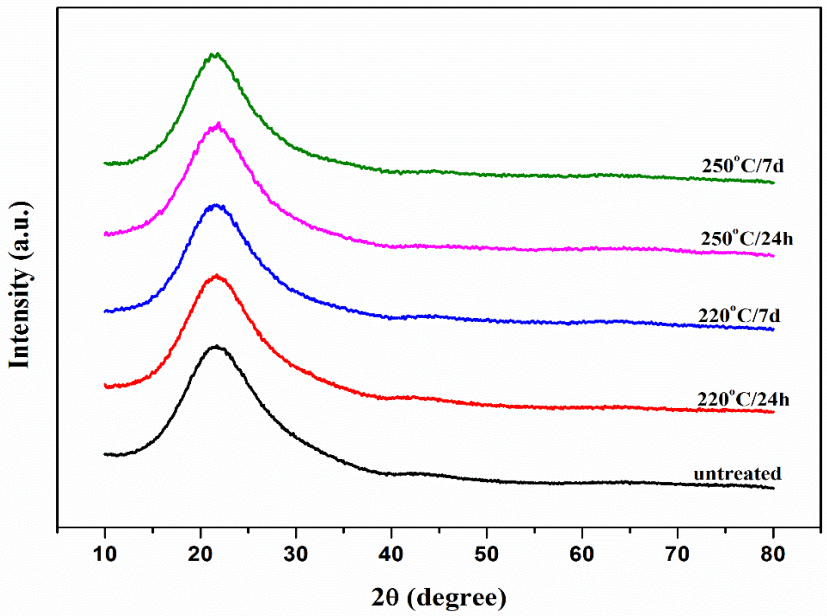

Figure A.3 pXRD diagram of untreated and treated SA277/0.1 samples

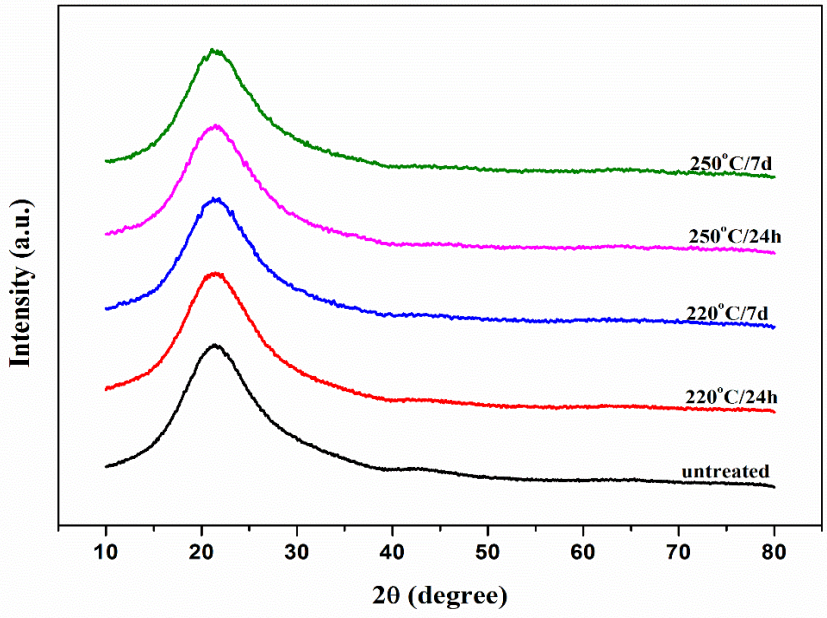

Figure A.4 pXRD diagram of untreated and treated ST54/1.0 samples

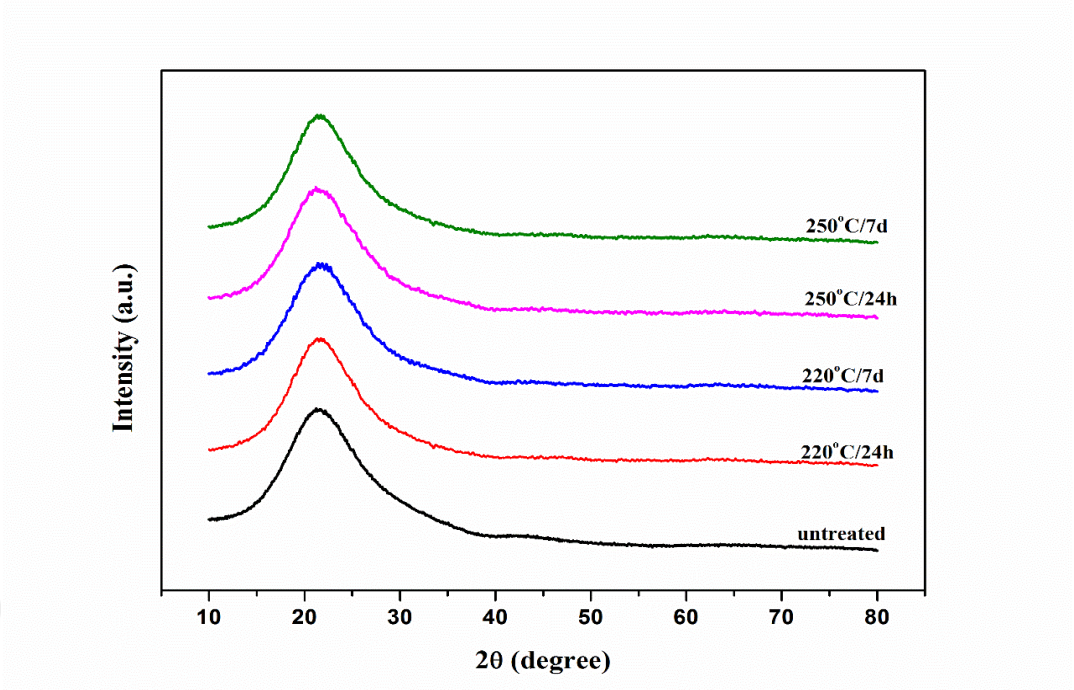

Figure A.5 pXRD diagram of untreated and treated ST196/0.9 samples

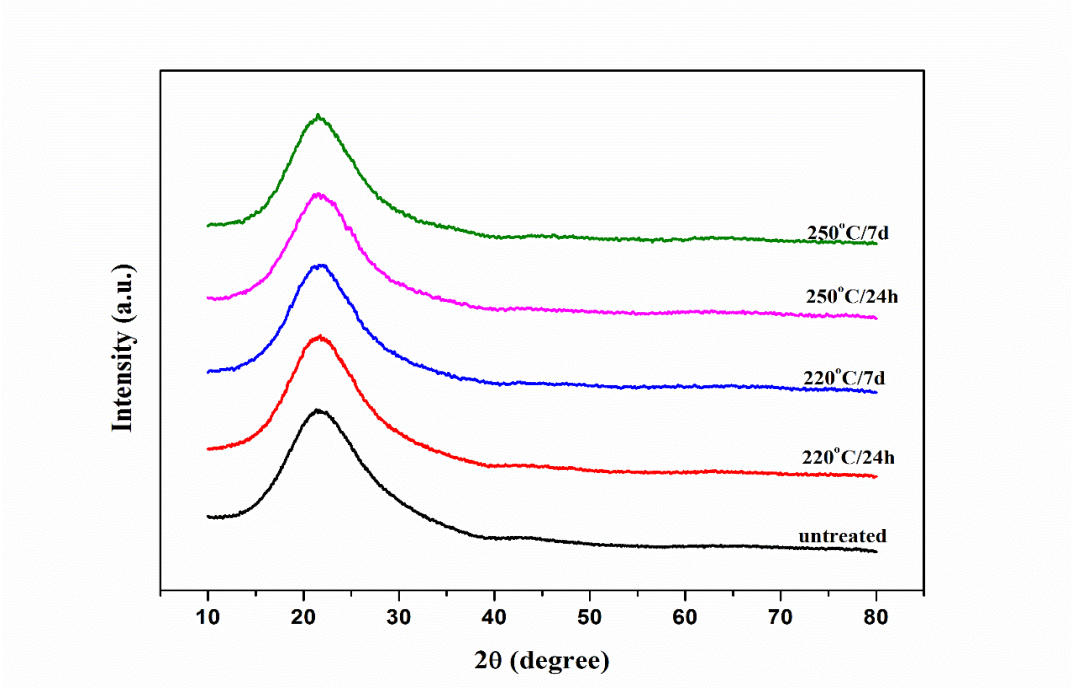

Figure A.6 pXRD diagram of untreated and treated ST313/0.8 samples

B. SEM Images of the Samples

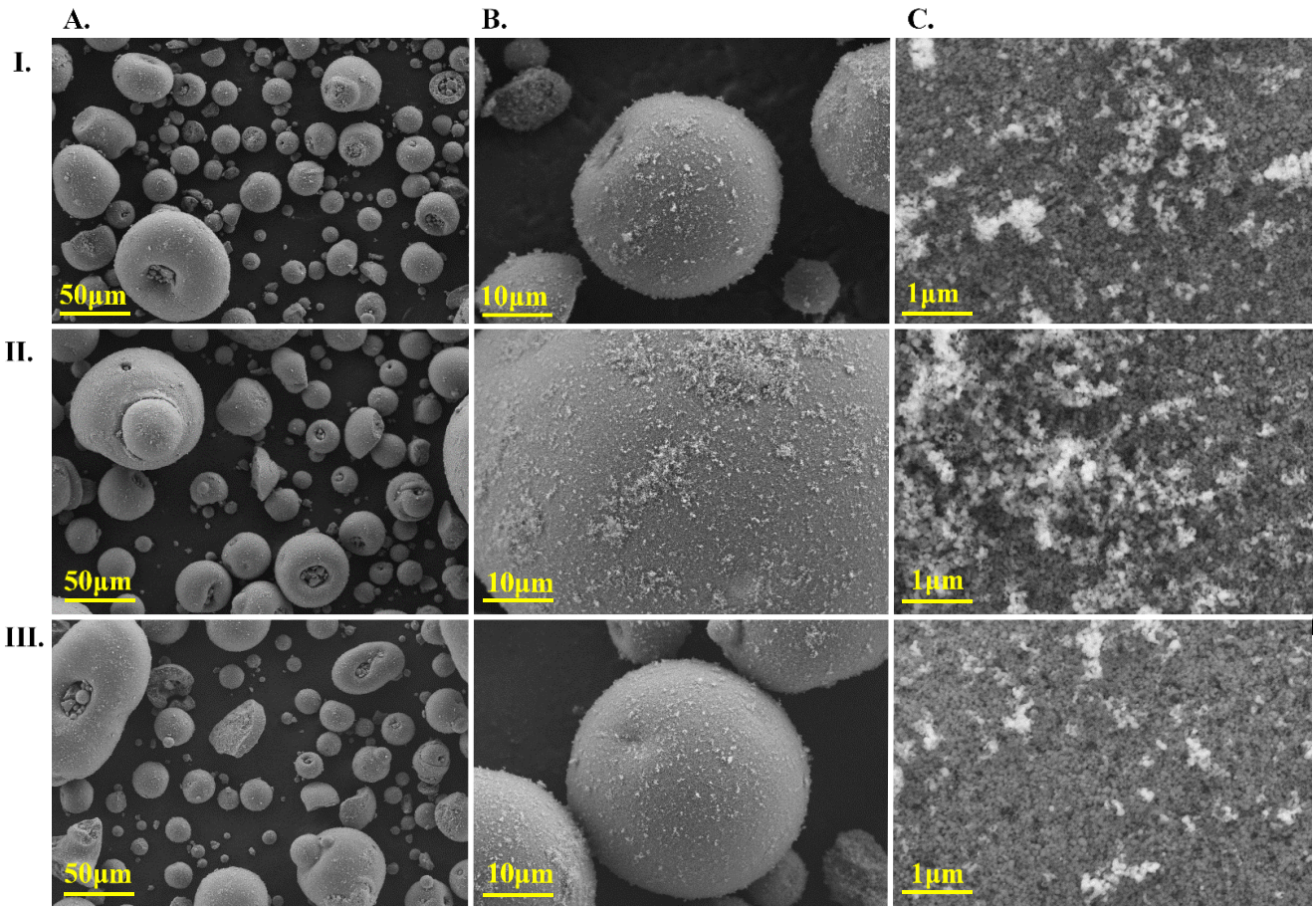

Figure B.1 SEM images of untreated (I.) and treated (II. 220°C/7d & III. 250°C/7d) SA65/0.5 samples with different magnifications (A. 1.00KX, B. 5.00KX, C. 50.00KX)

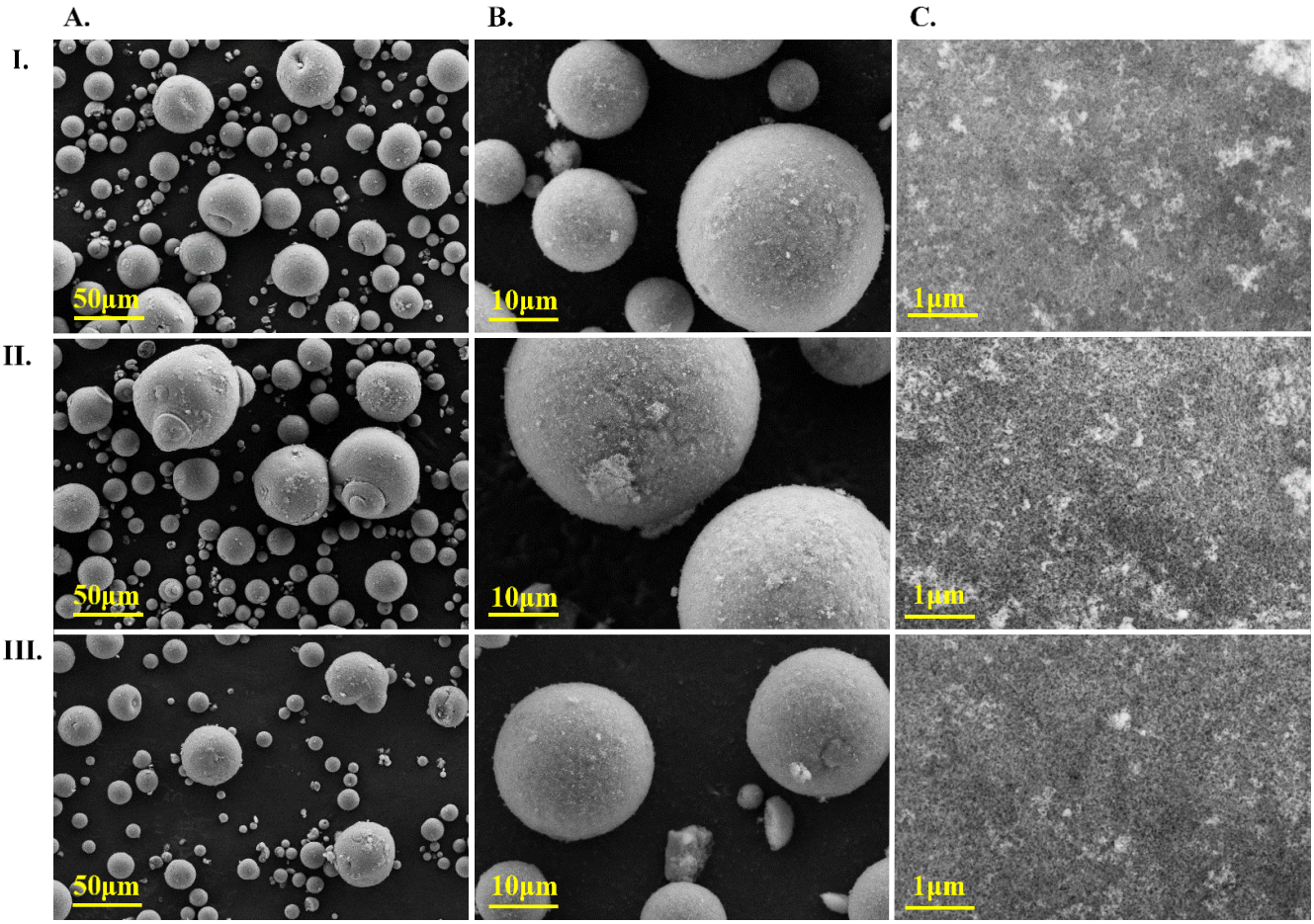

Figure B.2 SEM images of untreated (I.) and treated (II. 220°C/7d & III. 250°C/7d) SA277/0.1 samples with different magnifications (A. 1.00KX, B. 5.00KX, C. 50.00KX)

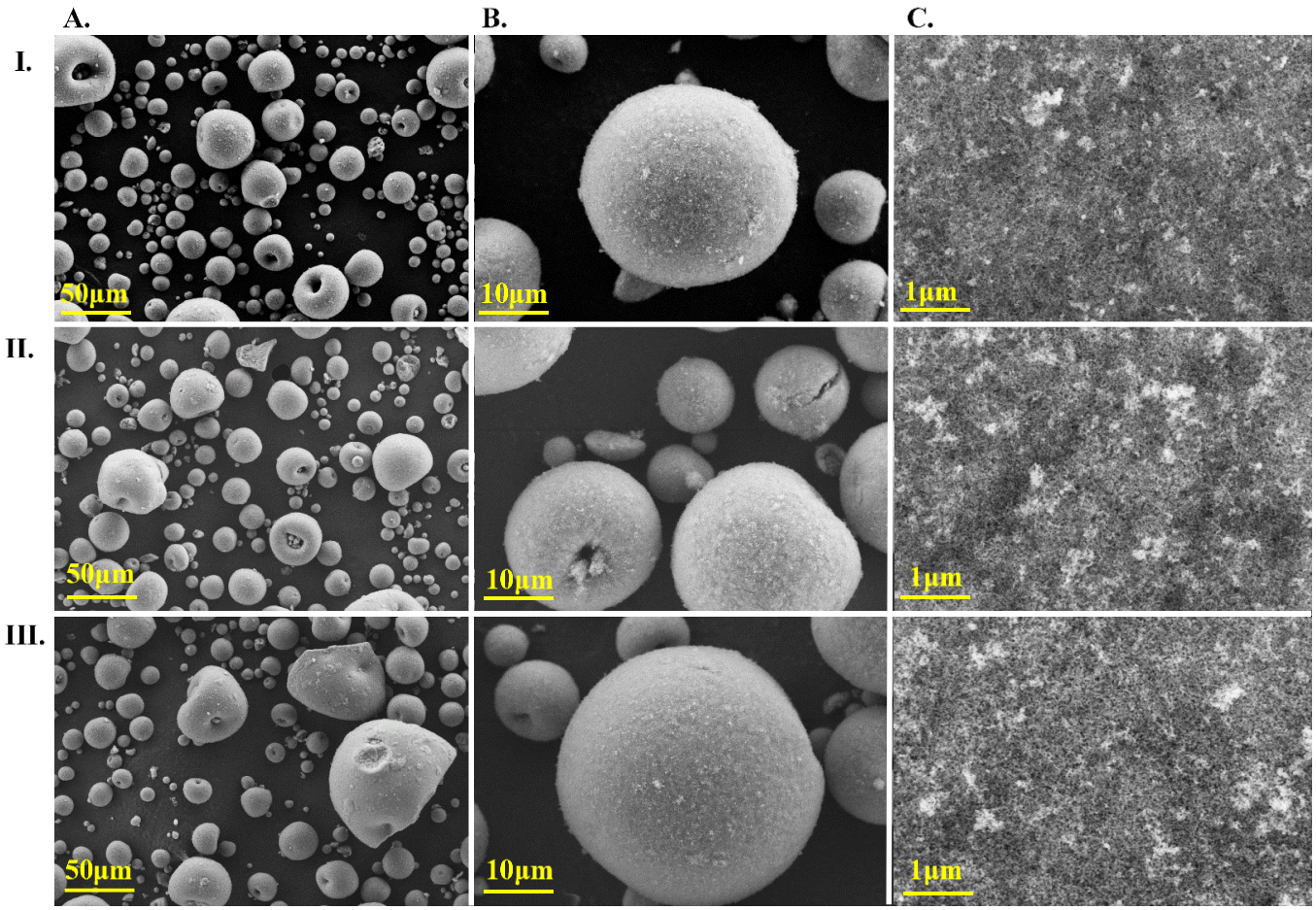

Figure B.3 SEM images of untreated (I.) and treated (II. 220°C/7d & III. 250°C/7d) ST196/0.9 samples with different magnifications (A. 1.00KX, B. 5.00KX, C. 50.00KX)